

SSC DETECTOR SOLENOID DESIGN NOTE #39

TITLE: Conceptual Design Studies of Large Solenoids

AUTHOR: Shigeki Mori, Institute of Applied Physics, Univ of Tsukuba

DATE: Feb 1, 1990

ABSTRACT: Conceptual design studies of a large superconducting solenoid proposed by the Large Solenoid Group at the 1987 Berkeley Workshop (the LSD solenoid) were carried out with the cooperation of Hitachi, Ltd. The solenoid has a bore diameter of 8.6 m, a length of 16 m, and a stored magnetic energy of 1.6 GJ with a central field of 2 T. Fully stabilized AMY-type superconductor is used with a pool-boiling cryostat arrangement. The design allows the solenoid to quench without being damaged. We demonstrate that such a magnet can be constructed with a modest extension of the existing superconducting technology. The feasibility of transportation of the magnet was also investigated in the event of construction of the solenoid carried out outside the SSC laboratory.

Shigeki Mori

Institute of Applied Physics
University of Tsukuba

Conceptual design studies of a large superconducting solenoid proposed by the Large Solenoid Group at the 1987 Berkeley Workshop (the LSD solenoid) were carried out with the cooperation of Hitachi Ltd. The solenoid has a bore diameter of 8.6 m, a length of 16 m, and a stored magnetic energy of 1.6 GJ with a central field of 2 Tesla. Fully stabilized AMY-type superconductor is used with a pool-boiling cryostat arrangement. The design allows the solenoid to quench without being damaged. We demonstrate that such a magnet can be constructed with a modest extension of the existing superconducting technology. The feasibility of transportation of the magnet was also investigated in the event of construction of the solenoid carried out outside the SSC laboratory.

1. INTRODUCTION

Preliminary results of conceptual design studies on a large superconducting solenoid, the LSD solenoid, proposed by the Large Solenoid Group at the 1987 Berkeley Workshop [1] have been reported [2]. Results of similar studies performed by a Fermilab group have also been reported [3]. In the LSD the entire section of the calorimetry except for the very forward region is placed inside the solenoid in order to provide continuous and hermetic coverage of the calorimetry. Although the solenoid becomes substantially larger compared with other arrangements [4], there is essentially no limitation in material thickness for the solenoid. Therefore, it can utilize fully stabilized, cryostable superconducting cables with a pool-boiling cryostat arrangement.

The earlier results by the two groups indicate that such a large solenoid with a stored electromagnetic energy of greater than 1 GJ can be constructed with a reasonable extension of the existing technology.

In the present report we summarize the results of studies done in Japan during the past two years with the cooperation of Hitachi Ltd.

2. GENERAL CHARACTERISTICS OF THE LSD SOLENOID

Fig.2-1 shows the schematic side and end views of the LSD. The calorimeter in the rapidity range of ± 3 is placed inside the central magnet system of a solenoid and a return yoke. The main parameters of the solenoid are given in Table I. The bore diameter is 8.6 m and the overall length is 16 m. The total stored energy is 1.6 GJ with a central field of 2 Tesla. Some of these parameters are slightly different from those given in Ref.2 because an additional space between the barrel calorimeter and return yoke is provided for a supporting structure of the calorimeter of about 5000 t in the present design. The magnet consists of eight identical modules of 1.84 m in length.

The schematic drawings of the solenoid arrangement are shown in Figs.2-2 and 2-3. Fig.2-4 depicts the schematic diagram of the power supply and control dewar arrangement. Each module has an independent power supply, but a single control dewar is shared by the eight modules. An arrangement of two cryostats is shown in Fig.2-4 in which each cryostat contains four modules and is connected to the common control dewar by a single chimney. As will be discussed in later sections, an arrangement having a single cryostat is very attractive from the stand point of the supporting system of axial electromagnetic forces.

The forced-flow cooling method has been used in large, thin superconducting solenoids of collider experiments [5]. This method is advantageous with regard to electrical insulation. On the other hand, since the pool boiling method can be arranged to be much stable against quenches, we chose

the pool-boiling method. One of the important criteria in the present design is that the solenoid must be safely recoverable in case of a quench which may occur in an emergency situation such as a failure of the refrigeration system.

3. COIL

3.1 Conductor

In the previous design we used the AMY conductor which satisfies cryostable conditions for the design current of 5000 A [6]. In the present design various design options for the conductor and current were considered.

The safety requirements we impose for the coil during quenches are as follows:

- (a) The maximum temperature rise T_{\max} must be less than 100 K.
- (b) The maximum voltage V_{\max} must be less than 1000 V.

For a short while after the protection circuit is activated during a quench, the resistivity of a normal section of the coil is small and the voltage rise induced in the normal section is negligibly small compared with the voltage appeared across the protection resistor. In general, the maximum voltage corresponds to the voltage across the protection resistor immediately after the protection circuit is activated. Therefore, if the protection resistor is grounded at the middle, the voltage to ground is reduced to one half of the voltage across the protection resistor. Nevertheless, our requirement is that $V_{\max} < 1000$ V.

In this section we use the hot spot model to evaluate the requirements for the conductor to satisfy the above conditions.

The model predicts the following relation

$$\gamma \int^{T_{\max}} \frac{C}{\rho} dT = \frac{E_0 J_0^2}{V_{\max} I_0} = \Gamma \quad (1)$$

where γ , C , and ρ are respectively the density, specific heat, and resistivity of the conductor, the variable T is temperature, I_0 and J_0 are respectively the coil excitation current and current density, given by $J_0 = I_0/A$, A being the cross section area of the metal part of the conductor, and E_0

is the coil stored energy, given by $E_0 = L I_0^2 / 2$, L being the coil inductance. The parameter Γ depends upon T_{\max} and the characteristics of the conductor and is estimated to be approximately $1 \times 10^{17} \text{ A}^2 \text{ s/m}^4$ for $T_{\max} = 100 \text{ K}$ in the case of an AMY-type conductor.

Figure 3-1 shows the relation between V_{\max} and I_0 for $J_0 = 30, 50, \text{ and } 70 \text{ A/mm}^2$ and $T_{\max} = 100 \text{ K}$ when each module has an independent power supply. We choose conservatively $J_0 = 50 \text{ A/mm}^2$ and $I_0 = 6400 \text{ A}$ as the design parameters. The values of $E_0 J_0^2$ are plotted in Fig.3-2 as a function of I_0 for the AMY, CDF, and FNAL 15ft Bubble Chamber (BC) magnets together with the present design. The lines correspond to constant V_{\max} values as indicated. Fig.3-3 shows the relation between the stabilizer cross section area and I_0 as a parameter of E_0 for $T_{\max} = 100\text{K}$ and $V_{\max} = 1000 \text{ V}$. The dot point indicates the present parameters. We note that J_0^2 is inversely proportional to E_0 when all the other parameters are fixed. The number of power supplies to operate the solenoid can be chosen arbitrarily by adjusting the value of the current density.

The criterion for complete cryogenic stability of a superconductor can be given by the following relation:

$$\alpha = \frac{\rho I^2}{P A q \beta} < 1 \quad (2)$$

where I is the current, P the perimeter of the conductor, q the thermal flux from the conductor surface, and β the fraction of the conductor surface exposed to liquid helium. The product $q\beta$ is the heat transfer rate. Eq.(2) can be rewritten as

$$I \leq \left(\frac{2q\beta}{\rho} \right)^2 \frac{1}{J_0^3} \frac{(1 + \eta)^2}{\eta} \quad (3)$$

where η is the aspect ratio of the conductor cross section given by $\eta = b/a$, a and b being respectively the short and long sides of the rectangular cross section of the conductor. Fig. 3-4 shows the relation between J_0 and I for $q\beta = 0.1$ and 0.4 W/cm^2 and $\eta = 1.0$ in two stabilizer configurations, namely copper alone and a combination of copper and pure aluminum with an area ratio of 1:1. For a large value of $q\beta$, copper stabilizer alone can be advantageous because of superior

mechanical strength of copper, but for small $q\beta$ values aluminum stabilizer must be added. In the case of the AMY solenoid $q\beta$ was measured to be 0.132 W/cm^2 .

Table II shows some examples of conductors considered in the present design study. The basic requirements for conductors are (1) complete stability, (2) mechanical strength, and (3) sufficiently large critical current. The compactness and the feasibility of fabrication of long unit lengths are also important requirements. The main parameters of the conductor we finally chose are given in Table III.

The stability factor of the present conductor is given by

$$\alpha = \frac{I^2}{q\beta P \left(\frac{A_{\text{Cu}}}{\rho_{\text{Cu}}} + \frac{A_{\text{Al}}}{\rho_{\text{Al}}} \right)} = 0.85 < 1$$

where $I = 6400 \text{ A}$, $q\beta = 0.132 \times 0.9 \text{ W/cm}^2$ (10% safety factor), $A_{\text{Cu}} = 1.16 \text{ cm}^2$, $A_{\text{Al}} = 0.118 \text{ cm}^2$, $\rho_{\text{Cu}} = 3 \times 10^{-8} \text{ }\Omega\text{cm}$, $\rho_{\text{Al}} = 0.3 \times 10^{-8} \text{ }\Omega\text{cm}$, and $P = 5.2 \text{ cm}$. Thus the conductor is shown to be cryostable.

3.2 Modules and Electromagnetic Properties

The solenoid consists of 8 identical modules of 1.84 m in length. The main parameters of the solenoid module are given in Table IV. Each module weighs about 68 t. Each coil is made of 6 layers of the AMY-type conductor winding discussed in the previous section and has in total 540 turns.

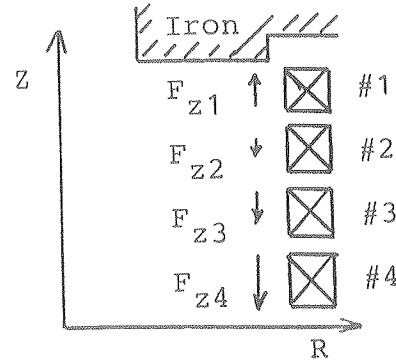
Figure 3-5 shows a magnetic flux distribution calculated by the finite element analysis program (Newton-Rapson method). The central field is 2.1 Tesla and the local maximum field at the coil is about 2.5 Tesla. A calculated flux distribution without the iron return yoke is shown in Fig.3-6 for an excitation current of 6400 A. The central and maximum fields are 1.9 and 2.7 Tesla, respectively.

Figure 3-7 shows the designed short-sample magnetic flux versus critical current relation. The load line drawn corresponds to the maximum flux of 3 Tesla. The maximum load is comfortably 62 % of the short sample data.

Electromagnetic forces exerted on the coils were calculated in the arrangement shown below. The other four

coils hold the symmetric forces with respect to the solenoid center.

Coil	F_r (10^3 t)	F_z (10^3 t)
#1	10.6	0.777
#2	11.3	-0.133
#3	11.1	-0.633
#4	10.5	-2.49



When four modules are connected in series in a two-cryostat arrangement, the cumulative axial force becomes 2480 t in the direction toward the solenoid center.

The maximum average radial hoop stress is given by

$$\sigma_h = \frac{F_r / n}{2 \pi S} = 26 \text{ kg/mm}^2$$

where n is the number of turns in a module, given by $n = 540$, and S is the conductor cross section, given by $S = 128 \text{ mm}^2$. Similarly, in the axial direction the maximum average stress is estimated to be $\sigma_z = 1.8 \text{ kg/mm}^2$ which is comfortably small.

As will be described later, Fig.3-8 shows the cryostat arrangement in which two cryostats with four modules each are connected at the middle to form a single unit. Compared with the arrangement with two separate cryostats, the cumulative axial force can be arranged to be cancelled out in the single cryostat arrangement. Thus the axial support system becomes relatively simple. Figs.3-9 and 3-10 show the schematic drawings of details of the conductor winding arrangement. Coil winding of 6 layer conductors can be made with the double pancake method or the solenoid winding method. Since the former method requires large numbers of pancake units and also conductor joints, one joint for every double pancake section, we decided to choose the solenoid winding method in which only one conductor joint is needed for a layer. Cooling channels and FRP insulation layers between conductors can be seen. The spacer ratio of the insulation layer to cooling channel in the axial direction is arranged to be about 70 %. The outer cylinder of a helium vessel made of SUS and a completed coil unit are assembled by the shrink-fit method. Fig.3-11 shows

the schematic drawing of the arrangement of the vacuum chamber, an axial support, the LN₂ thermal radiation shield, and the liquid helium cryostat.

A conductor joint is made at each end of a layer and no joint is made in the middle section. Fig. 3-12 shows measured data of the joint resistance as a function of the joint length. For example, the joint resistance is about $2 \times 10^{-9} \Omega$ for a joint length of 30 cm at 4.2 K and 0 T.

A design example of the module joint is shown in Fig.3-13.

4. CRYOSTAT

4.1 Vacuum Vessel

We consider an arrangement with two separate cryostats in this section as shown on the right side. Design parameters are:

(1) Requirements

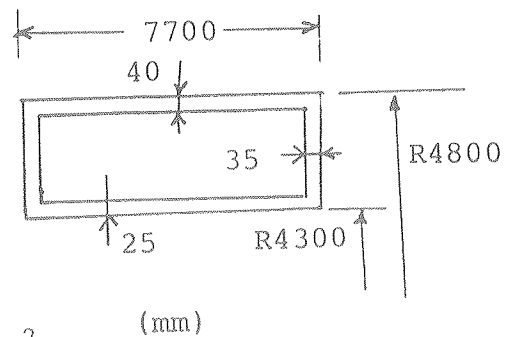
- a) Inner pressure 0.01033 kg/mm^2
- b) Reverse pressure 0.004 kg/mm^2

(2) Dimensions and structure

See the figure.

(3) Material

SUS304, $\sigma_{al} = 14 \text{ kg/mm}^2$



We will show that the outer and inner cylinders and the side plates shown in the figure satisfy safety requirements.

Outer cylinder

a) Stress in the circumferential direction:

$$\sigma = qR/t = 0.01033 \times 4782.5/40 = 1.2 \text{ kg/mm}^2 < \sigma_{al}$$

b) Buckling:

The critical pressure P_k is given by

$$P_k = 0.807 \frac{E}{(1 - \nu^2)^{3/4}} \frac{t^2}{L R} \sqrt{\frac{t}{R}}$$

$$= 0.073 \text{ kg/mm}^2$$

where $E = 21000 \text{ kg/mm}^2$ and $\nu = 0.3$. Then, the safety factor S is given by $S = 0.073/0.01033 = 7.0 > 3$. Therefore, it is a safe design. We note that the safety factor is greater than 3 even for a single cryostat arrangement of 16 m in length with a cylinder of 40 mm in thickness.

Inner cylinder

a) Stress in the circumferential direction:

$$\sigma = qR/t = 0.01033 \times 4300/25 = 1.8 \text{ kg/mm}^2 < \sigma_{al}$$

b) Buckling:

Using the same formula as used in the outer cylinder, we have $P_k = 0.026 \text{ kg/mm}^2$ and $S = 0.026/0.004 = 6.5 > 3$. Again, even for a single cryostat arrangement the present design is safe.

Side plates

A side plate can be approximated by a long plate of 435 mm (= 500-40-25) in width supported at both edges. Then the maximum bending moment M is given by $M = PW^2/8 = 0.01033 \times 435^2/8 = 244 \text{ kg}$ and the maximum bending stress σ given by $\sigma = M/(t^2/6) = 1.2 \text{ kg/mm}^2 < \sigma_{al}$. Therefore, the present design is safe.

Calculations were made for a ring-shaped plate by using various formulas. These results are very consistent with those obtained above using the simple model.

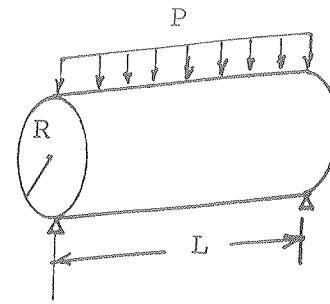
4.2 Calorimeter Support

As shown in Fig.2-1, a barrel calorimeter of about 5000 t is installed inside the solenoid. The outer diameter is 8 m and the length is 16 m. We consider two supporting schemes shown in Fig.4-1, namely (A) a support cylinder and (B) a pair of rectangular pillars. Firstly we do simple calculations by using formulas in simple models in order to make the first guess on which scheme is better. We will show that the cylinder scheme is more desirable. Secondly we perform detailed studies using the finite element analysis program ADINA.

4.2.1 Simple Model Analyses

(A) Support cylinder

A support cylinder is attached on the return yoke. The inner cylinder of the vacuum vessel can be utilized as the calorimeter support. A model to calculate stresses and deformations is shown on the right side [7].



The stress is given by

$$\sigma = -1.217 B^{-1} P R^{1/4} L^{1/2} t^{-7/4}$$

where $B = \{12(1 - \nu^2)\}^{1/8}$, ν being Poisson's ratio and P is the weight per length, given by $P = 2\pi R \rho t + w$ (w : calorimeter weight). With $\nu = 0.33$, $R = 4100$ mm, $L = 16000$ mm, $\rho = 7.9 \times 10^{-6}$ kg/mm³, and $w = 5000 \times 10^3 / (16000 \times 2) = 156.3$ kg/mm, we have

$$\sigma = 186.0 t^{-3/4} + 142.8 \times 10^3 t^{-7/4}$$

Fig.4-2 shows the relation between σ and t for $L = 16$ and 8 m. The latter corresponds to the case in which the calorimeter is additionally supported at the middle.

The deformation is given by

$$\delta = 0.0305 B^5 P R^{3/4} L^{3/2} t^{-9/4} E^{-1}$$

With $E = 21000$ kg/mm² we have

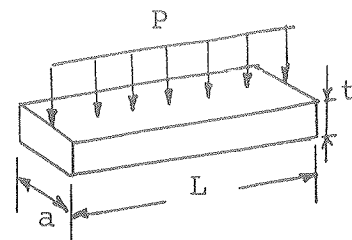
$$\delta = 1364 t^{-5/4} + 1048 \times 10^3 t^{-9/4}$$

The relation between δ and t is also shown in Fig.4-2.

Since the allowed stress of SUS304 is $\sigma_{al} = 14$ kg/mm², the required thickness of the support cylinder is 226 mm and the corresponding deformation is 6.8 mm.

(B) Rectangular pillars

Rectangular pillars are attached on the return yoke and support the calorimeter from the top and bottom sides. A model is shown on the right side.



The stress and deformation are given by

$$\begin{aligned}\sigma &= (P L^2/12) / (a t^2/6) \\ \delta &= P L^4 / (384 E a t^3/12)\end{aligned}$$

where $P = \rho a t + w$; $w = 156.3 \text{ kg/mm}$.

For $a = 2000 \text{ mm}$ we have

$$\begin{aligned}\sigma &= 6.4 \times 10^4 (0.0158/t + 156.3/t^2) \\ \delta &= 4.9 \times 10^7 (0.0158/t^2 + 156.3/t^3)\end{aligned}$$

Fig.4-3 shows the above two relations. For $\sigma_{al} = 14 \text{ kg/mm}^2$ the required thickness of a pillar is 880 mm and the corresponding deformation is 12 mm.

We conclude that the cylinder scheme is better than the pillar scheme in order to keep the support structure as compact as possible. High strength material such as SUS304N can be used to reduce the thickness of the support structure, but the amount of deformation can not be reduced.

4.2.2 FEM Analysis

Figure 4-4 shows the geometrical conditions used in the FEM analysis in which the cylinder support scheme is employed. We studied three different configurations at the connection of two cryostats and a support cylinder at the middle:

- (1) completely separated
- (2) combined together, and
- (3) combined together and attached to the return yoke.

Table V summarizes results of calculations. As expected, the last case gives the smallest values for the maximum stress and deformation. A combined arrangement of the inner vacuum wall of 25 mm in thickness and an additional support cylinder with a wall thickness of 125 mm can provide an adequate support for the calorimeter in configuration (2) which seems to be more flexible during installation work. The maximum stress and the maximum vertical displacement are respectively 11.2 kg/mm^2 and 2.1 mm in this case. Further optimization can be made after details of the mechanical structure of the calorimeter system become available.

4.3 Coil Support System

The coil support system holds the weight of the cold mass and axial and radial magnetic forces. In an arrangement of two separate cryostats the cumulative axial magnetic force toward the solenoid center is estimated to be about 2480 t. (See Section 3.2.) On the other hand, if all 8 modules are connected mechanically in a single cryostat, axial forces are only due to magnetic decentering forces and estimated to be about 70 t for a displacement of 13 mm. In this section we consider the arrangement of two cryostats. The schematic drawing of the support system is shown in Fig.4-5. Schematic side and end views of individual axial and radial supports are shown in Figs.4-6 and 4-7, respectively. Design parameters of the axial and radial support systems are as follows:

Axial support

Net magnetic force	2550 t
Number of support rods per cryostat	18
Support rod	
Material	Inconell 718
Allowed stress	43.4 kg/mm ²
Inner/outer diameters	70/100 mm
Length	1000 mm
Maximum design stress (tension)	35.4 kg/mm ²
Thermal leak per cryostat	
LHe	33.5 W
LN ₂	688 W

Radial support

Weight	180 t
Decentering magnetic force	50 t
Number of support rods per cryostat	12 x 2
Support rod	
Material	Inconell 718
Allowed stress:	
Primary	43.4 kg/mm ²
Primary + secondary (thermal)	130.1 kg/mm ²
Diameter	40 mm

Length	1100 mm
Maximum design stress:	
Primary	26.4 kg/mm ²
Primary + secondary (thermal)	67.4 kg/mm ²
Thermal leak per cryostat	
LHe	16.9 W
LN ₂	139 W

4.4 Control Dewar

As shown in Fig.2-2, we propose to have a single control dewar which is common to all 8 solenoid modules and located on the top of the outside of the return yoke. Simplified schematic diagrams of the top and side views of the control dewar are shown in Fig.4-8. It has a liquid helium reservoir of 1500 l and 8 pairs of power leads.

5. QUENCH PROPERTIES

As described in Section 3, the superconductor was designed to satisfy various safety requirements in case the solenoid quenches for an unexpected reason. The maximum voltage and maximum temperature rise are kept respectively below 1000 V and below 100 K in the hot spot model in which the growth of the normal section of the coil due to a quench is not taken into account and also thermal diffusion from the normal section is neglected. In addition, the resistivity of the coil section is assumed to be negligible compared with the protection resistor. Thus, this model predicts rather conservative limits when the protection circuit is operational. As shown in Fig.6 of Ref.2, quench simulations which assume more realistic characteristics of superconducting solenoids give a lower maximum temperature rise at a fixed maximum voltage.

In the normal operation mode, when a quench starts in one of the eight modules, all the eight protection circuits are activated simultaneously by opening each dump switch. We studied various cases in which some of the protection circuits do not operate due to failures. Unfortunately, an arrangement of four power supplies, each for two adjacent modules, was used in

these simulations. Furthermore, a stored energy of 1 GJ which corresponds to the earlier design with a slightly smaller radius was assumed. Therefore, we note that the results of the present calculations are not exactly applicable to the final design presented in this report.

Figure 5-1(a) shows the schematic diagram of the power supply arrangement. We assume that a quench starts in the first coil section, #1. We also assume $I_0 = 6400$ A and a protection resistance of 0.15Ω . We consider the following three cases:

1. normal operation,
2. #1 protection circuit activated, but the other three protection circuits not activated, and
3. all 4 protection circuits not activated.

Figs.5-1(b), (c), and (d) show calculated current, internal voltage induced by the normal section, and maximum temperature rise as a function of time in the three cases in this order. Magnetic coupling between coils was taken into account. Some of results are summarized below.

Case	<u>t = 0 sec</u>	<u>t = 200 sec</u>				<u>t = 0 to 200 sec</u>	
	V_{ext} (V)	I_{max} (A)				T_{max} (K)	V_{int} (V)
		#1	#2	#3	#4		
1	960	650	1350	1350	1100	80	115
2	960	400	6750	6500	6400	58	60
3	0	1600	6800	6500	6400	220	970

V_{ext} is the voltage across the protection resistor immediately after the protection circuit is activated. Thus, $V_{ext} = 0$ V in case 3. The maximum temperature T_{max} and the maximum internal voltage V_{int} appear always in the section where a quench starts. In cases 2 and 3 the current in the adjacent coil section, #2, increases due to magnetic induction.

In case 3 the temperature rise and internal voltage indeed reach somewhat uncomfortable values. It should be, however, remembered that such a case is an extremely rare system failure. A temperature rise of 220 K can be tolerated without damages and an internal voltage of 970 V is still within the design limit.

Electromagnetic forces during a quench were calculated in various cases. They are not significantly different from those calculated under the normal operating conditions. (See Section 3.2.) No serious problems are anticipated.

The pressure rise of the helium vessel during a quench was calculated by using a model. Fig.5-2 shows the calculated pressure rise in the helium vessel as a function of the time after a quench. The blasting pressure of the relief cover is set at 3 kg/cm²G. The peak pressure in the vessel is roughly the same as the relief pressure of the blasting valve and no appreciable pressure difference is created. It implies that the pressure rise in the helium vessel during a quench can be controlled easily by the setting value of the relief pressure of the blasting valve.

6. MISCELLANEOUS

An estimated cool-down schedule of a module solenoid during tests is shown in Fig.6-1. It takes about 350 hours, about two weeks, before reaching liquid helium temperature from room temperature. The cool-down of the LSD solenoid requires a substantially longer period depending upon the cryostat arrangement.

The feasibility of transportation of the LSD solenoid from a Japanese maker to the SSC laboratory was investigated. Figs.6-2 and 6-3 illustrate an arrangement of a module during the overland transportation. It is concluded that the overland transportation in Japan and USA seems to be feasible at a reasonable cost. The transportation from Japan to USA will be made by a ship.

The possibility of on-site fabrication of the LSD solenoid was also studied. It turns out to be rather expensive because specialized large-scale instruments are required which may not be utilized for other jobs. Fig.6-4 shows a typical site-shop example which may allow efficient on-site construction.

Table VI shows an example of the construction schedule of the LSD solenoid. It must be remembered that it takes about five years.

7. CONCLUSIONS

A large, 2 Tesla superconducting solenoid magnet with a bore diameter of 8.6 m , a length of 16 m, and a stored magnetic energy of 1.6 GJ can be built with a reasonable extension of the existing superconducting technology. The magnet consists of 8 identical modules which are housed either in two separate cryostats or in a single cryostat. Each module is independently connected to an individual power supply through a common control dewar. Fully stabilized, cryostable AMY-type conductor is used with a pool-boiling cryostat arrangement.

Safety requirements during a quench are conservatively satisfied under the normal operating conditions. Even for unusual failures of the quench protection system the present design does not seem to have any fundamental safety problems. Further studies on failure modes are desirable to warrant the safety operation of the solenoid.

The arrangement with two separate cryostats requires a massive axial support system. A single cryostat configuration in which an axial support is required to hold only magnetic decentering forces must be investigated in detail regarding the assembly procedure, effects due to thermal contraction in the radial support system, and other items.

Fabrication of the LSD solenoid requires a number of specialized large-scale instruments and a large shop. Thus, on-site construction can be more expensive. In the case the solenoid is built by a Japanese maker, transportation of the solenoid to the SSC laboratory seems to be feasible.

Finally, we estimate that construction will take about five years without including on-site assembly and testing.

Acknowledgement

Cooperation by Hitachi Ltd. for the present design work of the LSD solenoid is acknowledged.

References

1. G. G. Hanson et al., "Report of the Large Solenoid Detector Group," Experiments, Detectors, and Experimental Areas for the Supercollider (World Scientific, Singapore, 1987), pp. 340-387.
2. S. Mori, "Preliminary Studies of Large Solenoids and Related Structure," High Energy Physics in the 1990s, Snowmass, 1988 (World Scientific, Singapore, 1989), pp. 837-840.
3. R. Fast et al., "SSC Detector Solenoid," High Energy Physics in the 1990s, Snowmass, 1988 (World Scientific, Singapore, 1989), pp. 841-844; R. Fast et al., Fermilab Internal Report TM-1620[SSC-N-663](September 1989), Fermilab, Batavia, IL, unpublished.
4. S. Mori, "HCD (Hermetic Collider Detector)," JSD Group Report (December 1989), unpublished; G. J. Feldman et al., "4 π Detectors," Proc. of the 1984 Summer Study on the Design and Utilization of the Superconducting Supercollider, edited by R. Donaldson and J. G. Morfin, Snowmass, CO (1984), p.624; D. Theriot et al., "4 π Detectors," Proc. of the 1986 Summer Study on the Physics of the Superconducting Supercollider, edited by R. Donaldson and J. Marx, Snowmass, CO (1986), p. 351.
5. For a summary report on large superconducting solenoids built recently see, for example, H. Hirabayashi, "Detector Magnets in High Energy Physics," IEEE Trans. on Magnetics, 24(1988)1256.
6. K. Tsuchiya et al., "A 3 Tesla Superconducting Solenoid for the AMY Particle Detector at TRISTAN," KEK Preprint 86-63, October 1986.
7. See, for example, R. J. Roark and W. C. Young, Formulas for Stress and Strain, McGraw-Hill Kogakusha, Ltd., 5th ed.

Figure Captions

- Fig. 2-1. Schematic side and end views of the Large Solenoid Detecor, LSD.
- Fig. 2-2. Schematic diagram of the side view of the LSD solenoid system with two chimneys and a single control dewar.
- Fig. 2-3. Schematic diagram of the end view of the LSD solenoid system with a single control dewar.
- Fig. 2-4. Schematic diagram of the cooling system arrangement of the LSD solenoid magnet with two independent cryostats. Each module is connected to an individual power supply through a common control dewar.
- Fig. 3-1. I_0 versus V_{\max} relation as a parameter of the current density J_0 for $E_0 = 200$ MJ, $T_{\max} (= \Delta T) = 100$ K, and $\Gamma = 1 \times 10^{17}$ A²sec/m⁴. The product $I V_{\max}$ is proportional to $E_0 J_0^2$.
- Fig. 3-2. I_0 versus $E_0 J_0^2$ relation for the FNAL BC magnet, the CDF and AMY solenoids, and the present design of the LSD solenoid with 8 power supplies, one for each module. The straight lines shown corresponds to constant maximum voltages for $T_{\max} (= \Delta T) = 100$ K and $\Gamma = 1 \times 10^{17}$ A²sec/m⁴.
- Fig. 3-3. Relation between E_0 and the stabilizer cross section area as a function of I_0 for $V_{\max} = 1000$ V and $T_{\max} (= \Delta T) = 100$ K. The dot point corresponds to the present design of 8 power supplies. The area is proportional to the square root of E_0 when all the other parameters are fixed.
- Fig. 3-4. Cryogenic stability condition for J_0 and I_0 as a parameter of the heat transfer rate $q\beta$. The solid and dashed curves correspond respectively to conductors with copper stabilizer and copper-pure aluminum stabilizer (1:1). The measured $q\beta$ value of the AMY conductor was 0.132 W/cm².
- Fig. 3-5. Calculated magnetic flux distribution. Local maximum fields are also indicated. The maximum field is 2.46 Tesla.
- Fig. 3-6. Calculated magnetic flux distribution in the case of no iron return yoke for an excitation current of 6400 A. The central and maximum fields are respectively 1.9 and 2.7 Tesla.
- Fig. 3-7. Magnetic flux versus critical current for a standard short sample. The load line corresponds to a conservative value of the maximum magnetic field experienced by the

conductor, 3 Tesla.

Fig. 3-8. Single cryostat arrangement. Two cryostats with four modules each are connected at the center to form a single cryostat. The dimensions shown with \times marks are very preliminary and will be optimized later.

Fig. 3-9. Schematic drawing of the side view of the coil cross section. An enlarged view shows the arrangement of the conductor and insulating layers.

Fig. 3-10. Cross section of the conductor and an enlarged view of the liquid helium cryostat and superconducting coil at the coil end.

Fig. 3-11. Schematic drawing of the end section of the cryostat where the axial coil support is installed. The dimension of the drawing is not scaled proportionally.

Fig. 3-12. Measured joint resistivity as a function of the joint length for the AMY conductor at 4.2 K and 0 T. The insert shows how a conductor joint is made by soldering with a copper spacer.

Fig. 3-13. Schematic diagram of a module joint.

Fig. 4-1. Calorimeter support method. (A)Support cylinder: the inner cylinder of the vacuum chamber or with an additional support cylinder fixed at the return yoke at the two ends of the solenoid. (B)Rectangular pillars: a pair of rectangular pillars located at the top and bottom sides of the calorimeter body fixed at the return yoke.

Fig. 4-2. Stress and deformation as a function of the cylinder thickness in the support cylinder method of the calorimeter support for support lengths of 8 and 16 m.

Fig. 4-3. Stress and deformation as a function of the thickness of a support pillar in the rectangular pillar method of calorimeter support for support lengths of 8 and 16 m.

Fig. 4-4. Geometrical arrangement used in the FEM analysis of the calorimeter support using the cylinder support method.

Fig. 4-5. Schematic section view of the axial and radial support system.

Fig. 4-6. Schematic side and top views of an axial support. The dimensions of the diagrams are not scaled proportionally.

Fig. 4-7. Schematic side and top views of sections of a radial support. The dimensions are in mm.

Fig. 4-8. Simplified schematic diagrams of the top and side views of the control dewar which is used for all the eight solenoid modules. Each module has a pair of individual power leads. Two chimneys are used in the bottom diagram.

Fig. 5-1(a) Schematic diagram of the quench protection circuit used in quench simulations. Two adjacent coils are connected in series to a power supply. The other figures show simulation results for $I_0 = 6400$ A, a protection resistance of 0.15Ω , and a stored magnetic energy of 1 GJ. The first coil section is assumed to start a quench at $t = 0$ sec. I_i represents the current in the i^{th} power supply circuit, $T_{1\text{max}}$ the maximum temperature of the first circuit, and R_n the resistance of the normal section of the first section. The results are obtained in the following three cases. (b) Normal operation in which all the four dump switches are opened immediately after the onset of the quench. The decay time of I_1 is the fastest among the four circuits because of the growth of the resistivity of the normal section R_n . The internal voltage, $R_n I_1$, reaches about 115 V. (c) #1 dump switch opened and the other three remained closed. The first two coils are turned off and the other six coils continue to operate. The maximum temperature and maximum voltage are comfortably low. (d) All the four dump switches remained closed. This case is the most serious because all the stored energy is dumped inside the source coil of a quench.

Fig. 5-2. Calculated pressure rise of the helium vessel during a quench. The relief pressure of the blasting valve is set at $3 \text{ kg/cm}^2\text{G}$.

Fig. 6-1. Estimated cool-down curve for a single module during a test. The mass flow rate is shown by dashed lines and temperature gradients are also shown.

Fig. 6-2. Arrangement for the overland transportation of a solenoid module. The overall height limit is 10 m.

Fig. 6-3. Arrangement for the overland transportation of a solenoid module. The overall height limit is 10 m.

Fig. 6-4. Typical site-shop for the on-site construction of the LSD solenoid.

Table I. Main parameters of the LSD solenoid

<u>Item</u>	<u>Parameter</u>
Bore diameter	8.6 m
Total length	16 m
Central field	2 Tesla
Number of modules	8
Number of cryostats	2 (or 1)
Total stored energy	1.6 GJ
Overall inductance	78 H
Total weight	540 t

Table III. Parameters of the LSD solenoid conductor

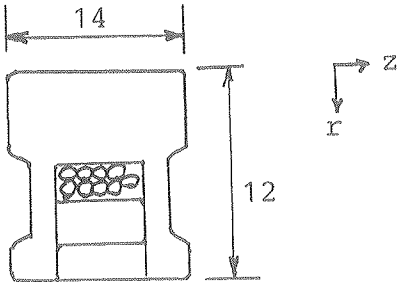
Item	Design value
Schematic diagram of the superconductor cross section and dimensions (in mm)	
Dimension	12 mm x 14 mm
Critical current	9000 A at 4.4T, 4.2K
Base conductor	
Material	Nb - 46.5wt% Ti
Filament diameter	30 μ m
Number of filaments	\approx 1013
Base conductor diameter	1.35 mm
Copper ratio	1.0
Twist pitch	30 mm
Strand	
Number of strands	9
Strand pitch	50 mm
Outer dimension	6.3 mm x 2.5 mm
Aluminum stabilizer coated with copper	
Outer dimension	6.3 mm x 2.7 mm
Copper area	25%
Resistivity of aluminum	$\leq 0.3 \times 10^{-8}$ Ω cm at 3 T
Copper stabilizer	
Material	Work-hardened, 1/2H
Resistivity	$< 3 \times 10^{-8}$ Ω cm at 3 T
Allowed stress (0.2%)	≥ 30 kg/mm ²
Area	
Copper	116.0 mm ²
Aluminum	11.8 mm ²
Equivalent electric resistivity	1.64×10^{-8} Ω cm at 3 T

Table IV. Main parameters of the solenoid module

<u>Item</u>	<u>Parameter</u>
Diameter (inner/outer)	8.6 m/9.6 m
Coil length	1.62 m
Current	6400 A
Central field	2 Tesla
Winding	
Number of layers	6
Total turns of winding	540
Stored energy	200 MJ
Cryostat: helium vessel	
Material	SUS304LN
Wall thickness (inner/outer)	37 mm/28 mm
Length	1.84 m
Conductor	AMY-type
Cold mass	49 t

Table V. Maximum stresses and displacements in the support cylinder of the central calorimeter calculated by the FEM analysis for the following three configurations at the connection of two cryostats at the joint:

Case A. two cryostats completely separated at the joint:

Case B. two cryostats connected together,

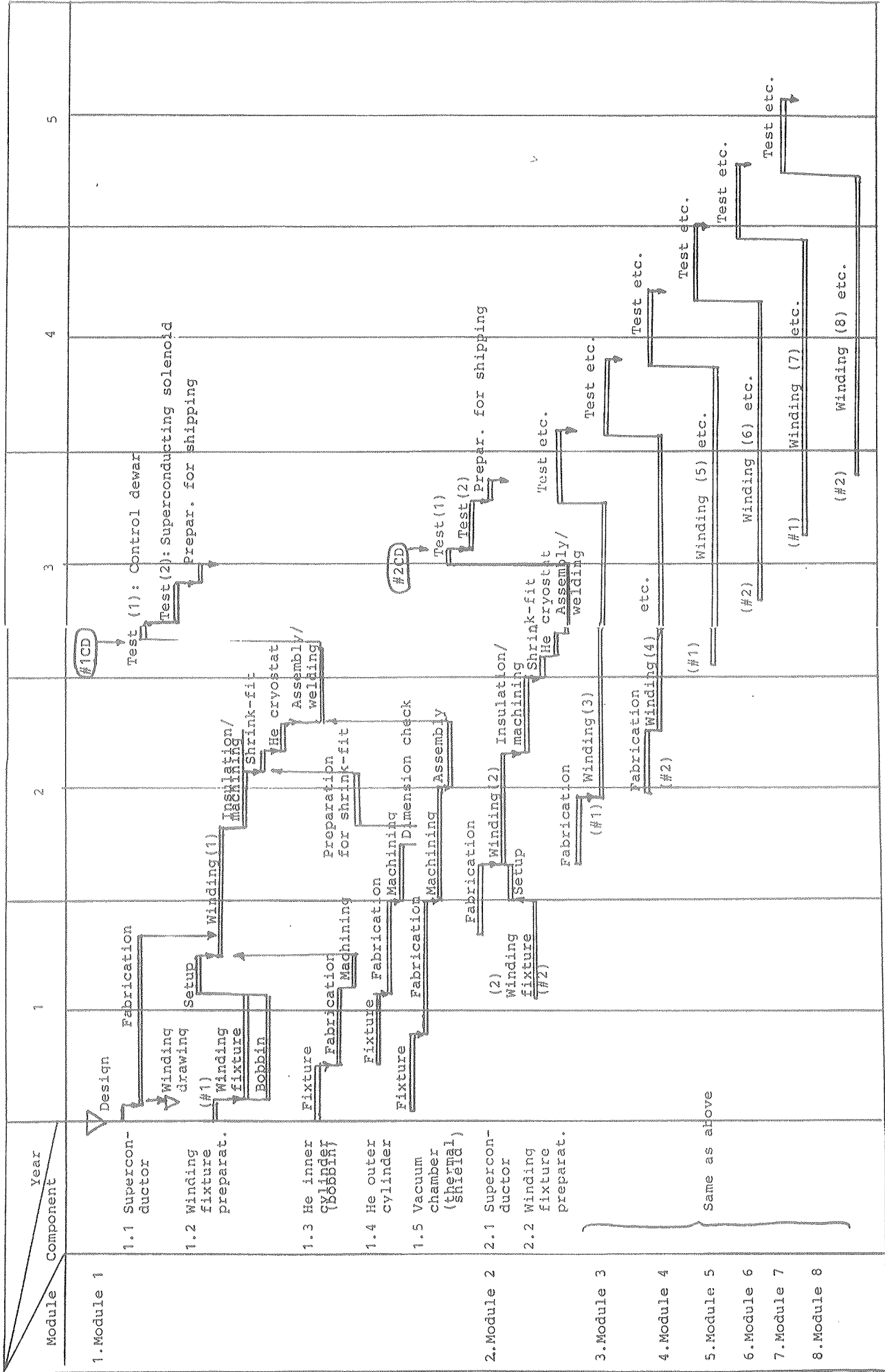
Case C. two cryostats connected together and fixed to the yoke at the joint.

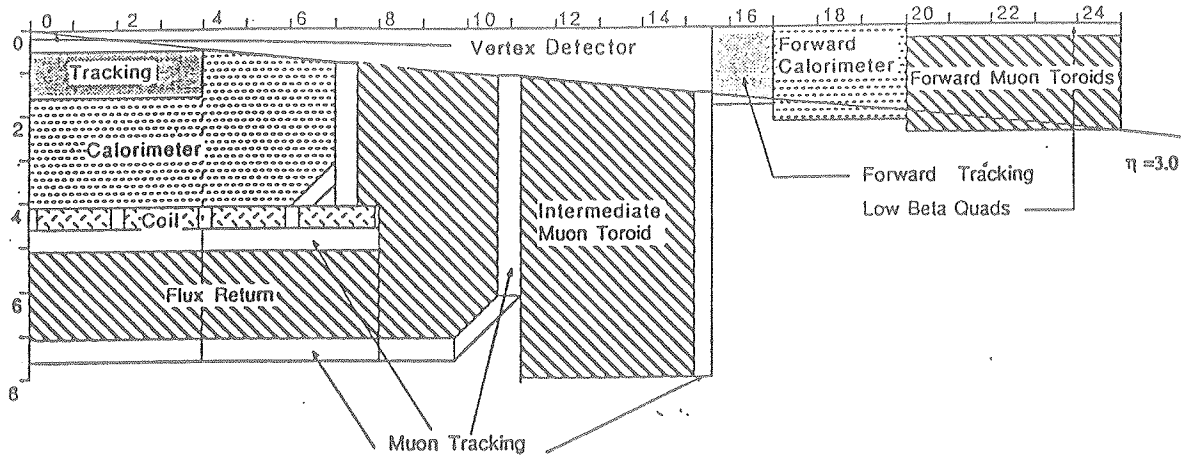
The support cylinder can be the inner vacuum cylinder alone or a combined system of the inner vacuum cylinder and an additional support cylinder. The weight of the calorimeter is 5000 t.

No	Case	Thickness (mm)		Maximum stress (kg/mm ²)	Maximum vertical displacement (mm)
		Inner vacuum wall	End plate		
1	A	25	35	33.0	11.7
2	B	25	35	29.8	8.9
3	C	25	35	23.6	5.8
4	C	25	100	17.4	5.8
5	C	25+75*	35	11.8	1.3
6	B	25	100	21.9	8.1
7	B	25+75*	35	17.1	3.0
8	B	25+125*	35	11.2	2.1

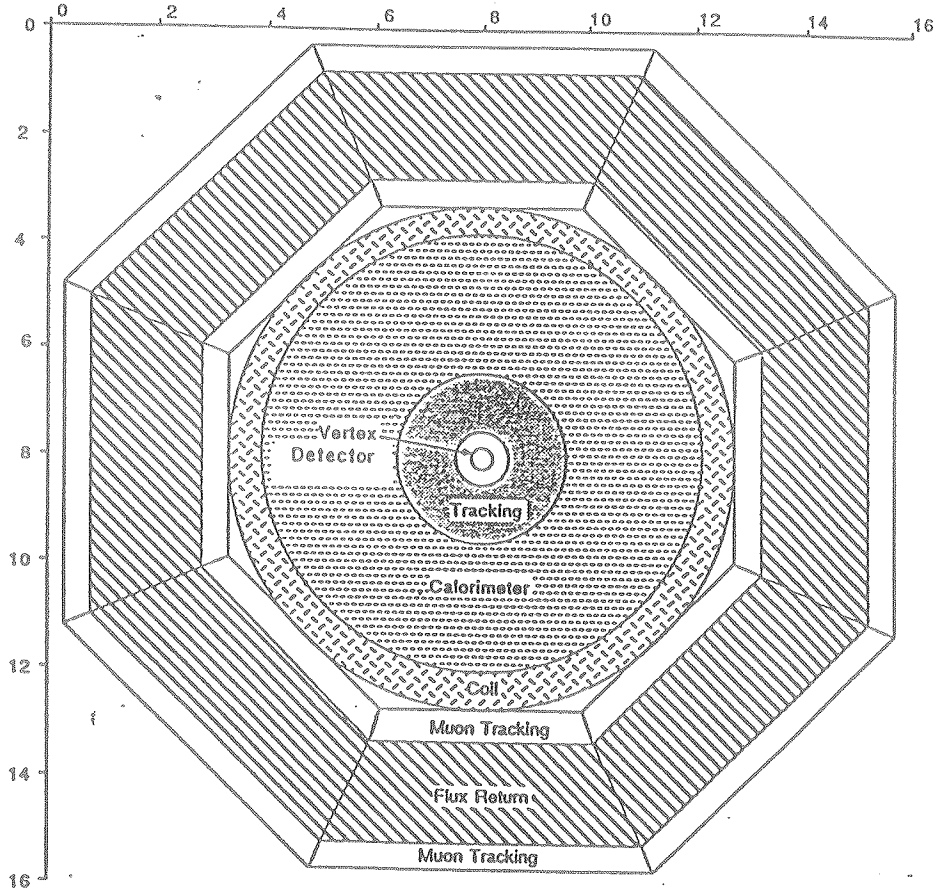
*The second figure corresponds to the thickness of an additional support cylinder. The thickness of the inner vacuum wall was assumed to be 25 mm in all the cases.

Table VI. Typical example of the construction schedule of the LSD solenoid.





(a)



(b)

Figure 2-1.

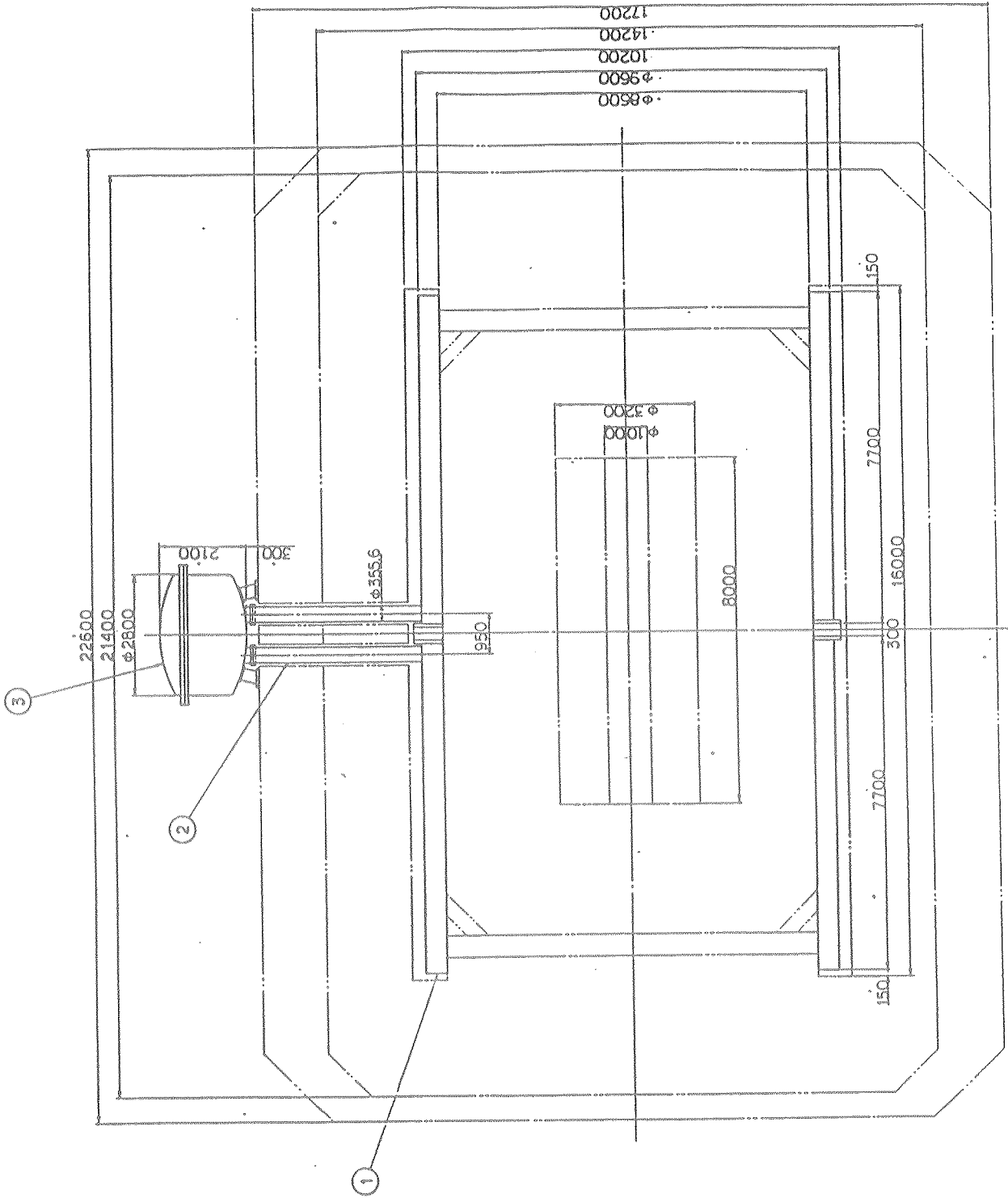


Figure 2-2.

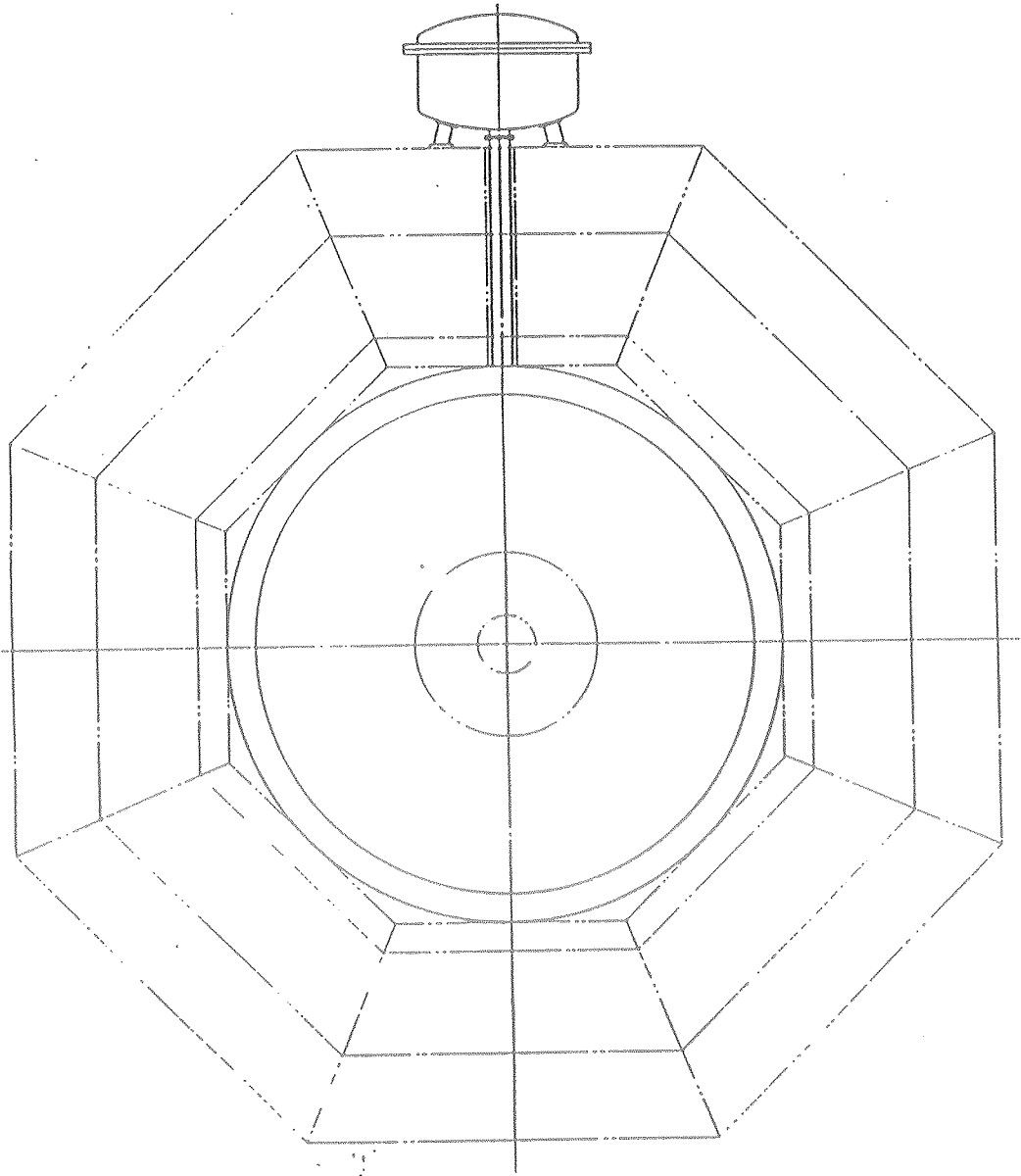


Figure 2-3.

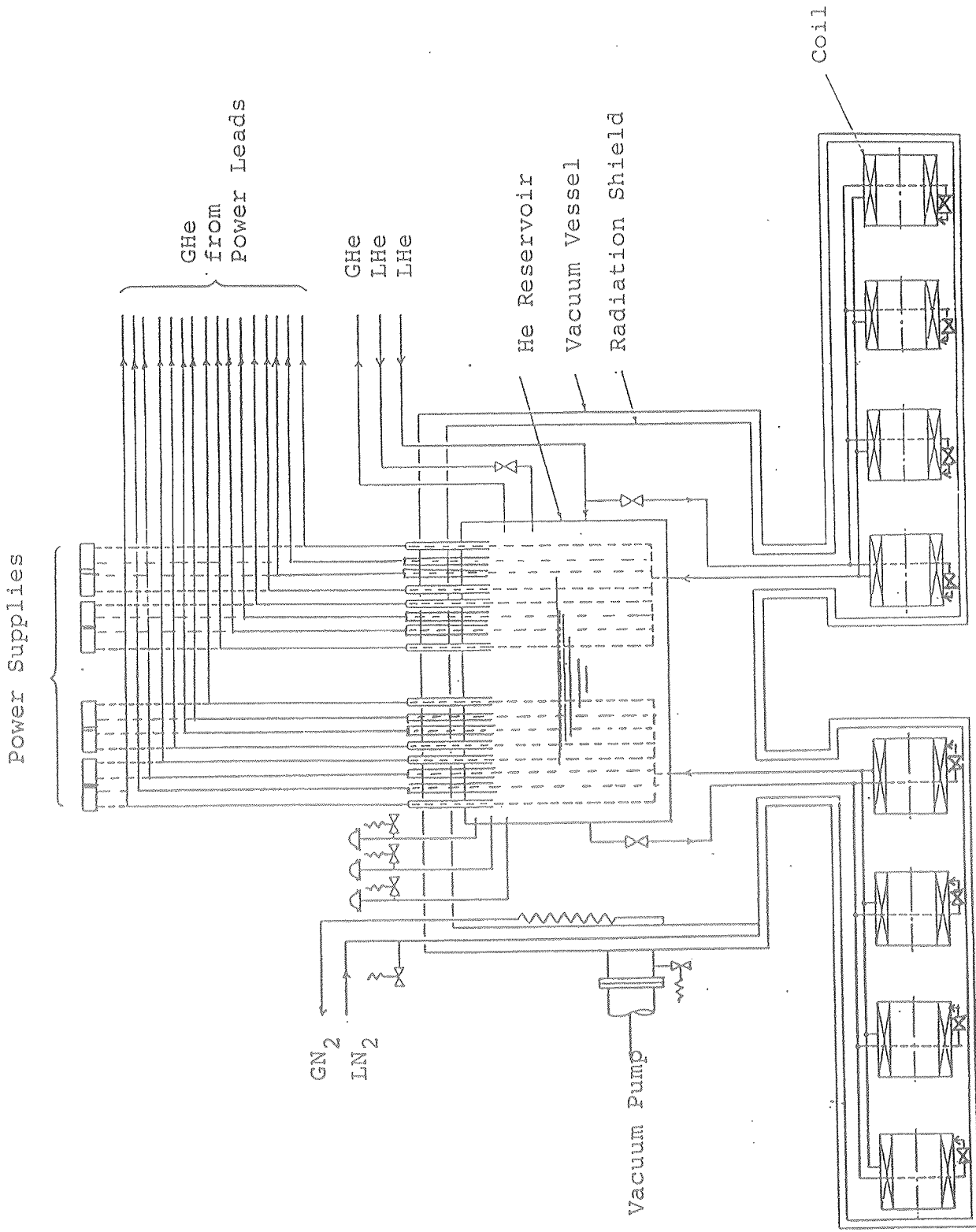


Figure 2-4.

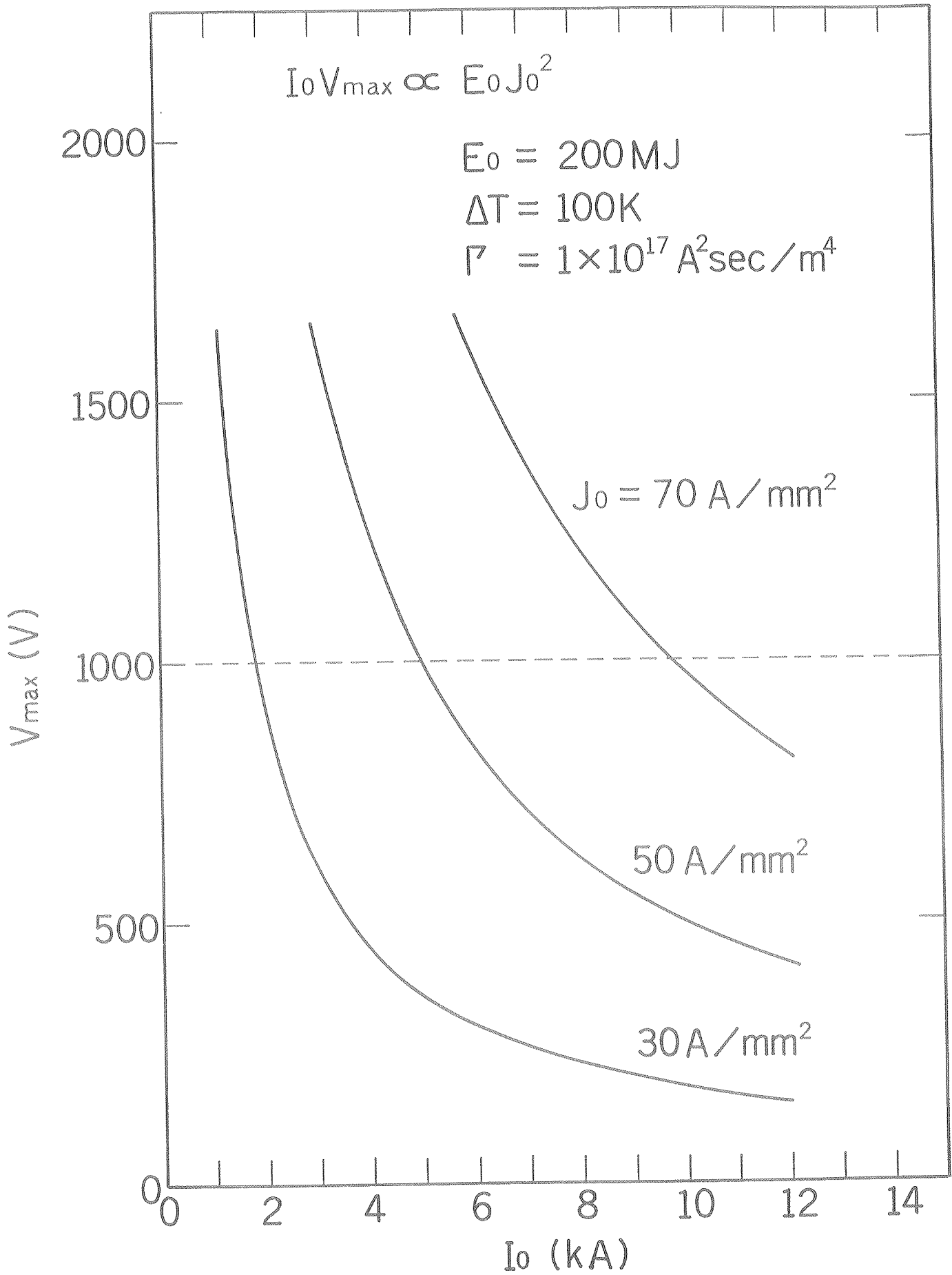


Figure 3-1.

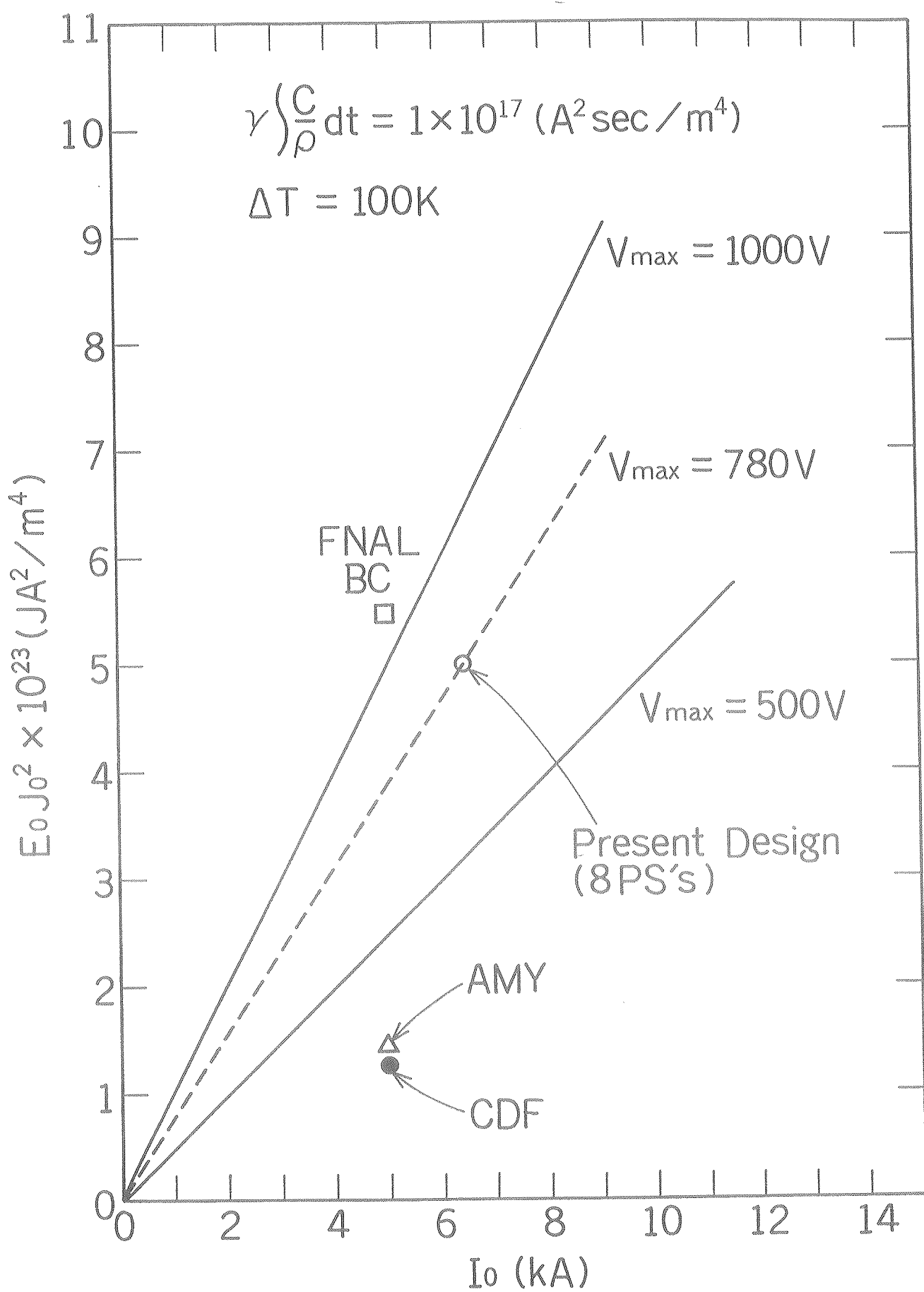


Figure 3-2.

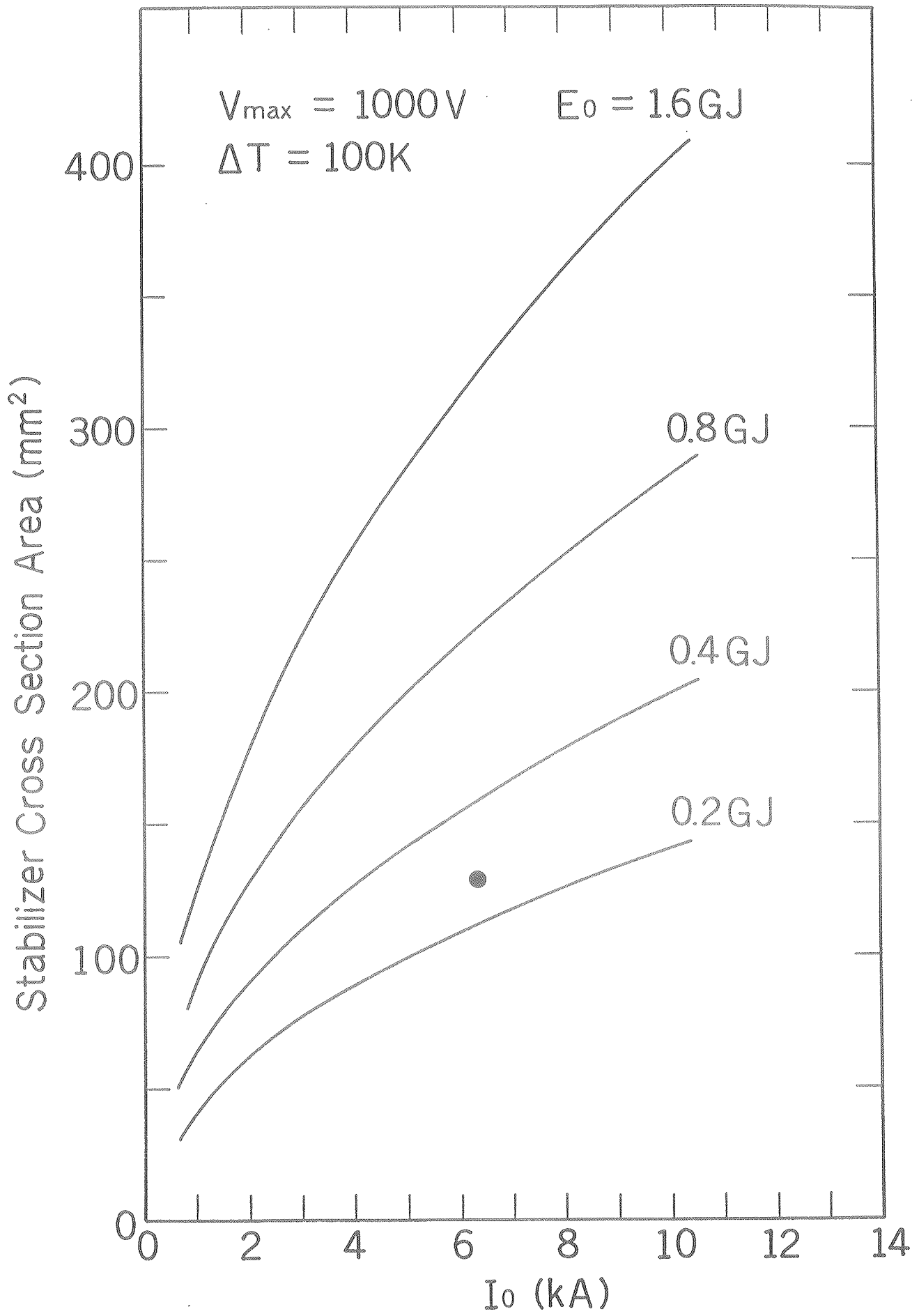


Figure 3-3.

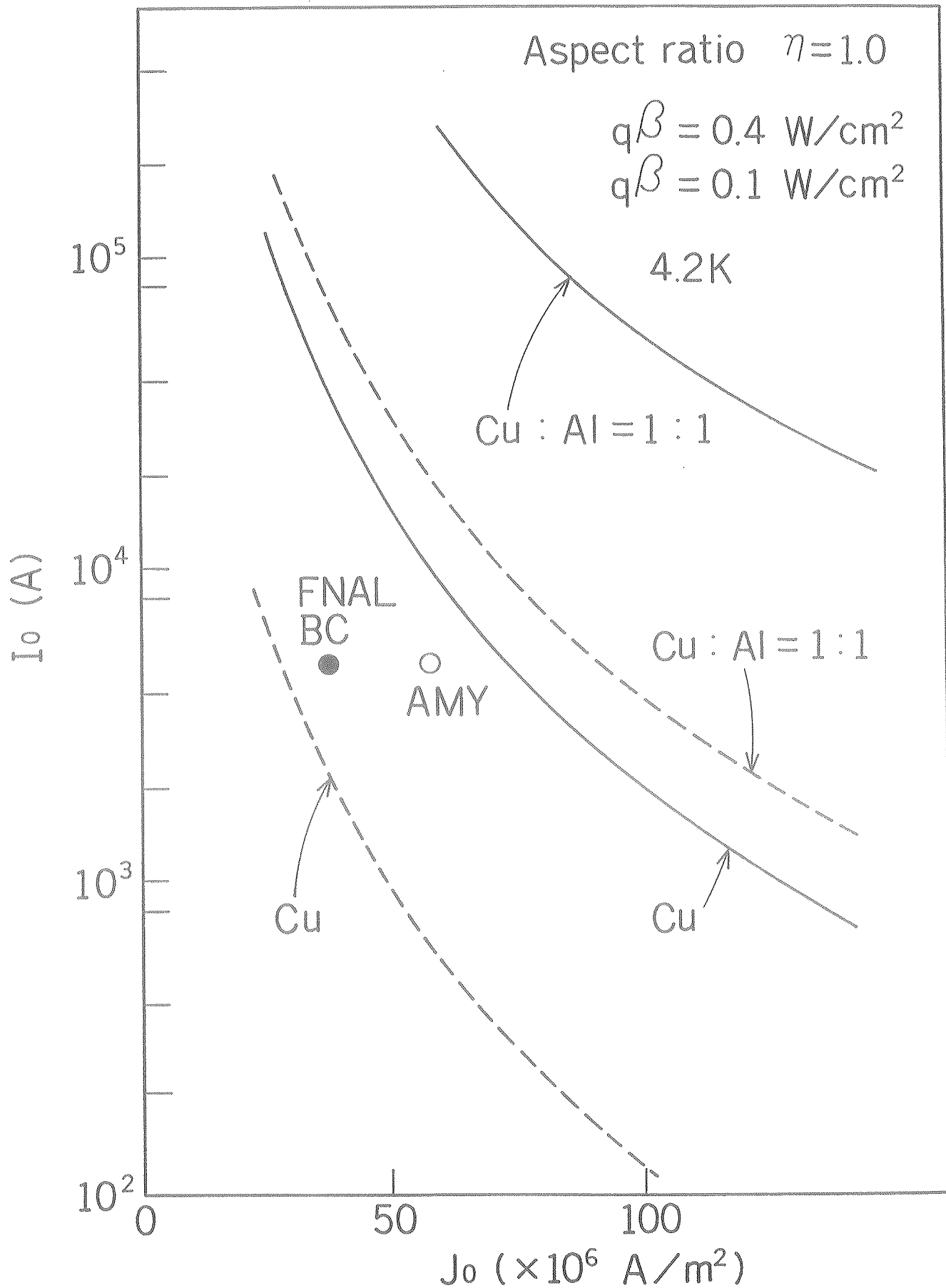


Figure 3-4.

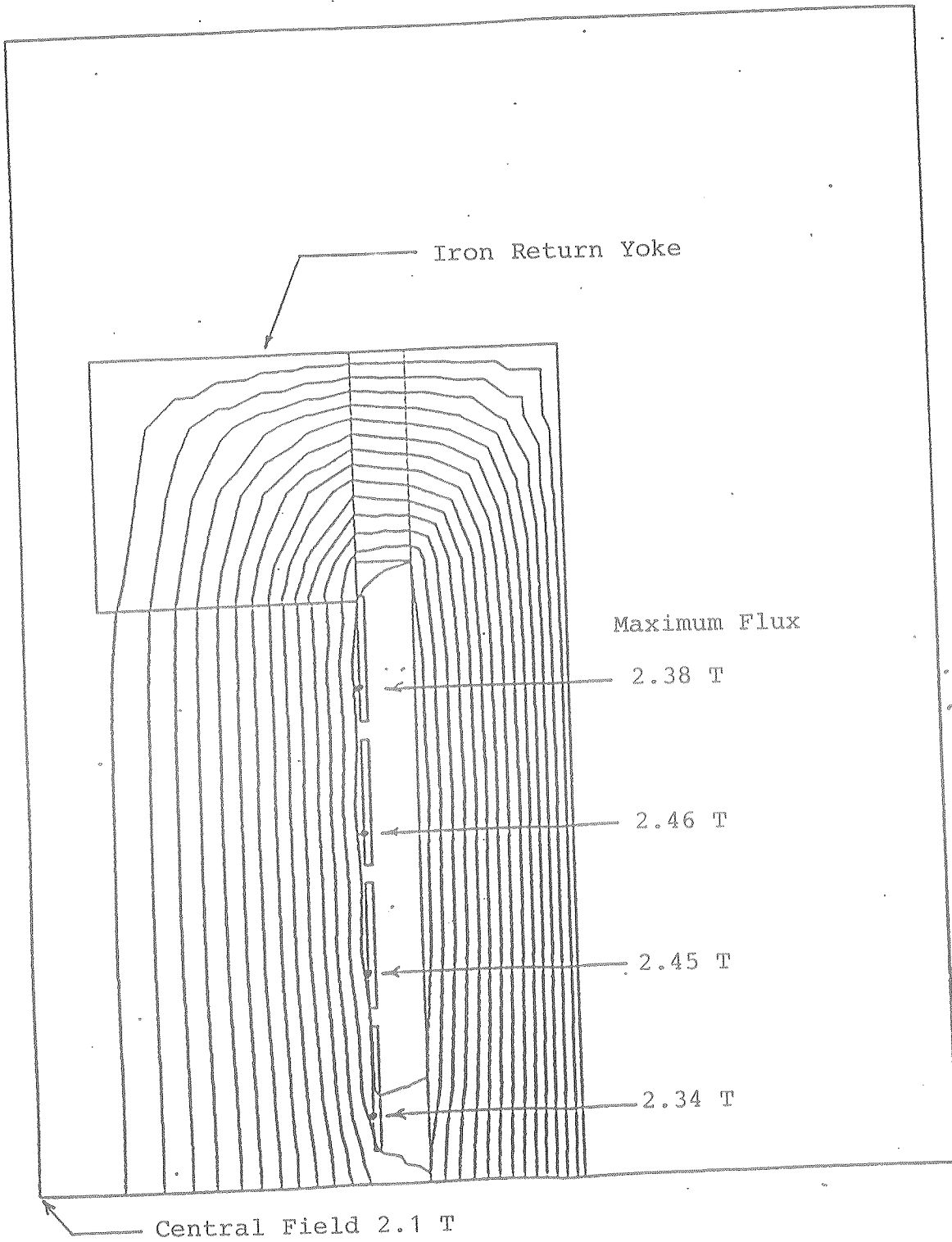


Figure 3-5.

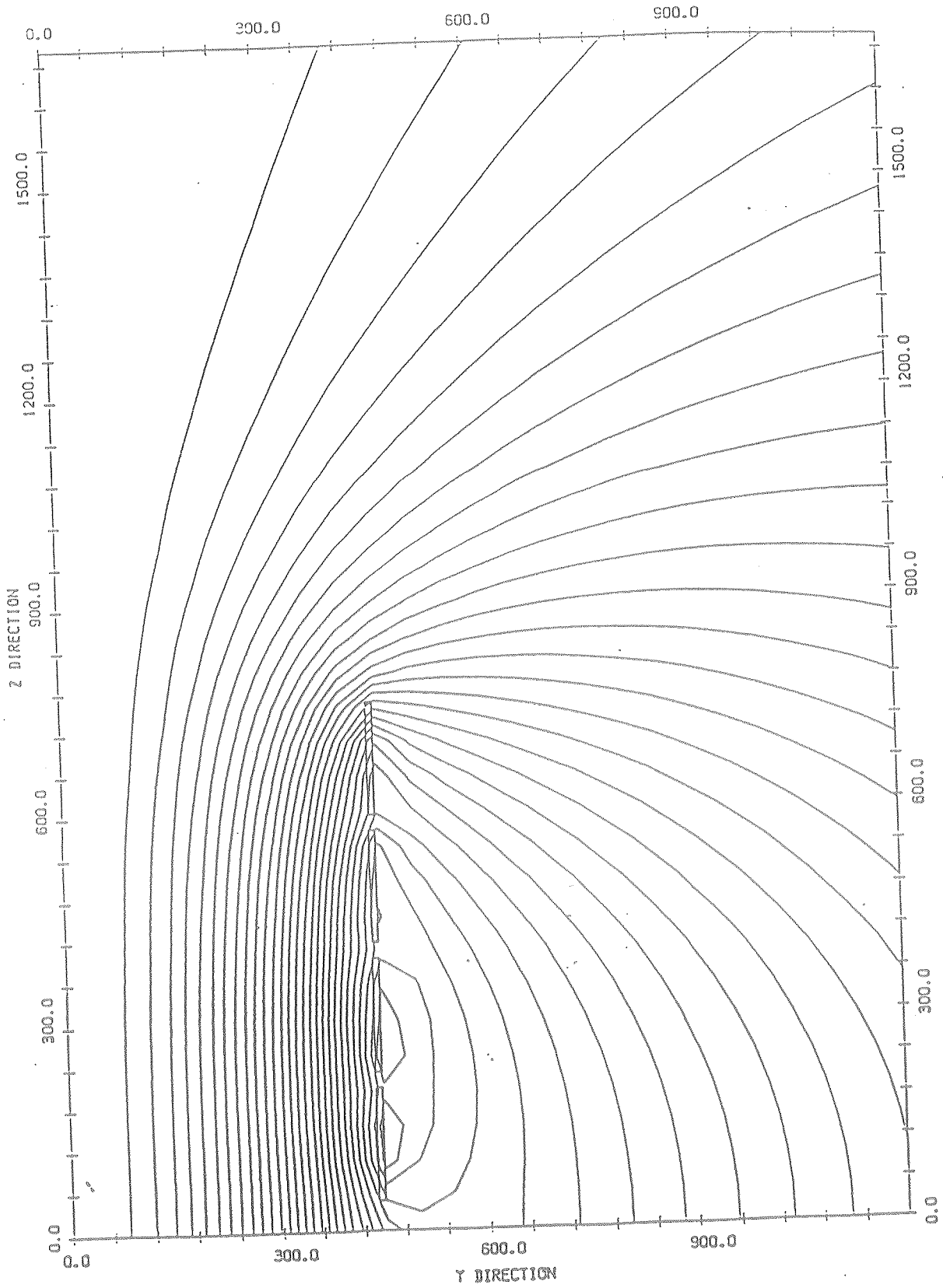


Figure 3-6.

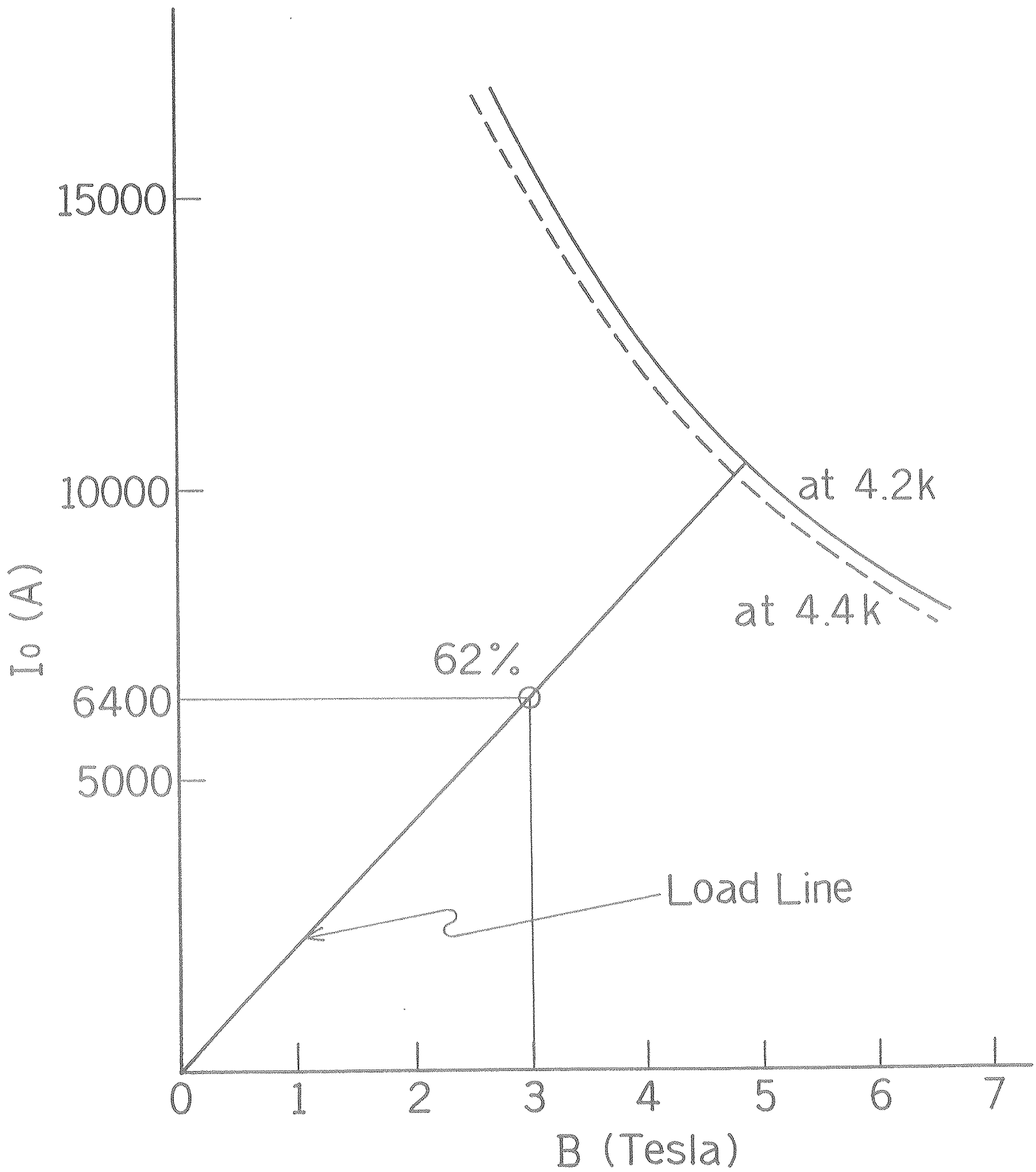


Figure 3-7.

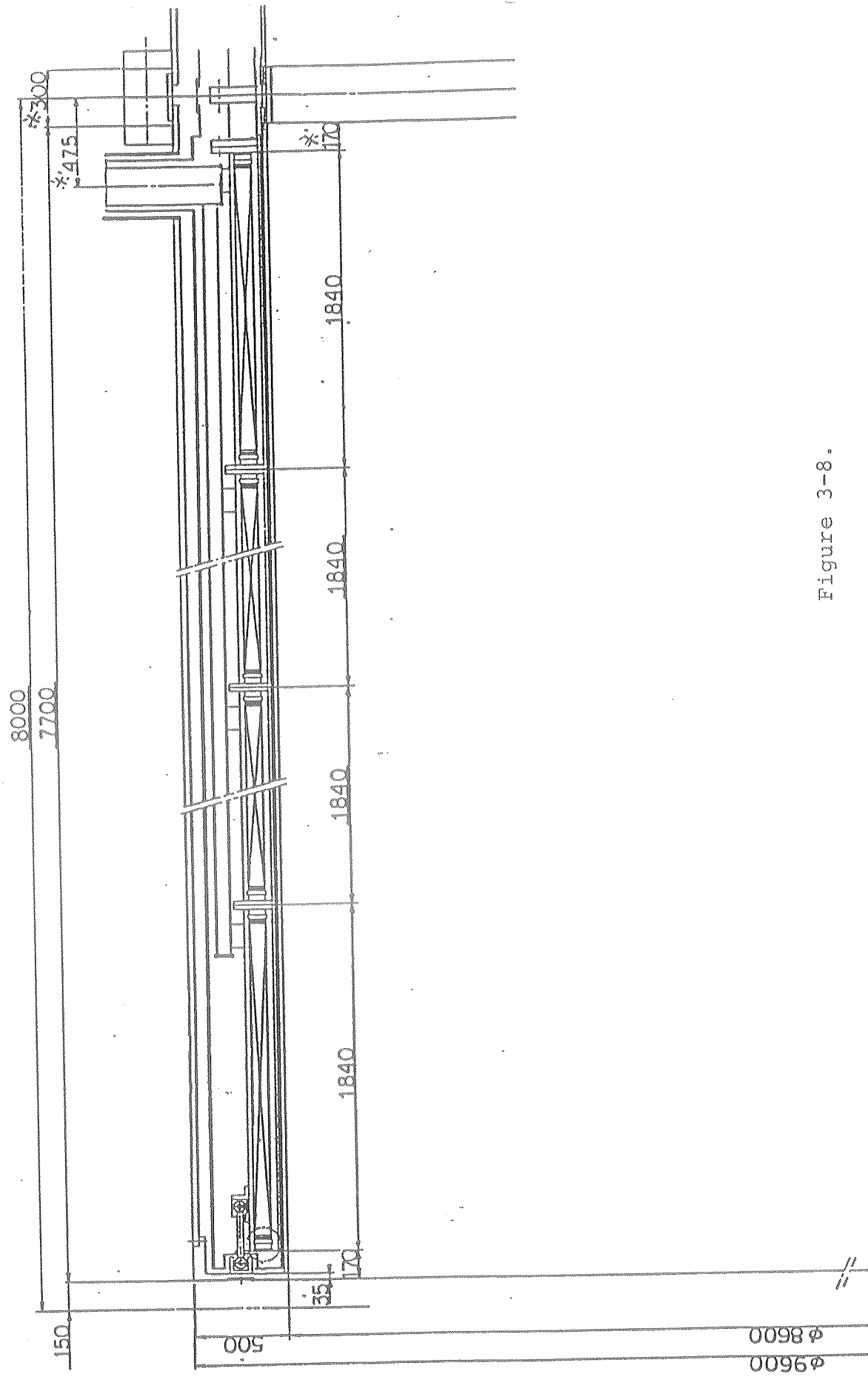


Figure 3-8.

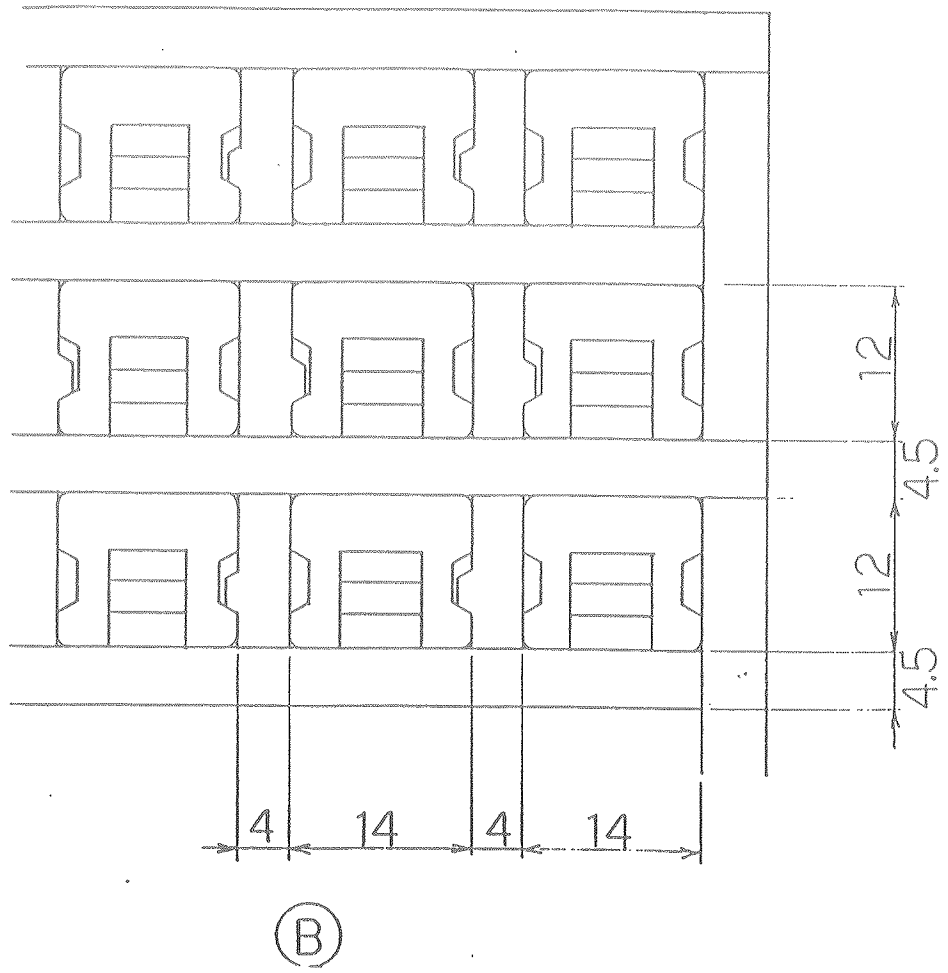
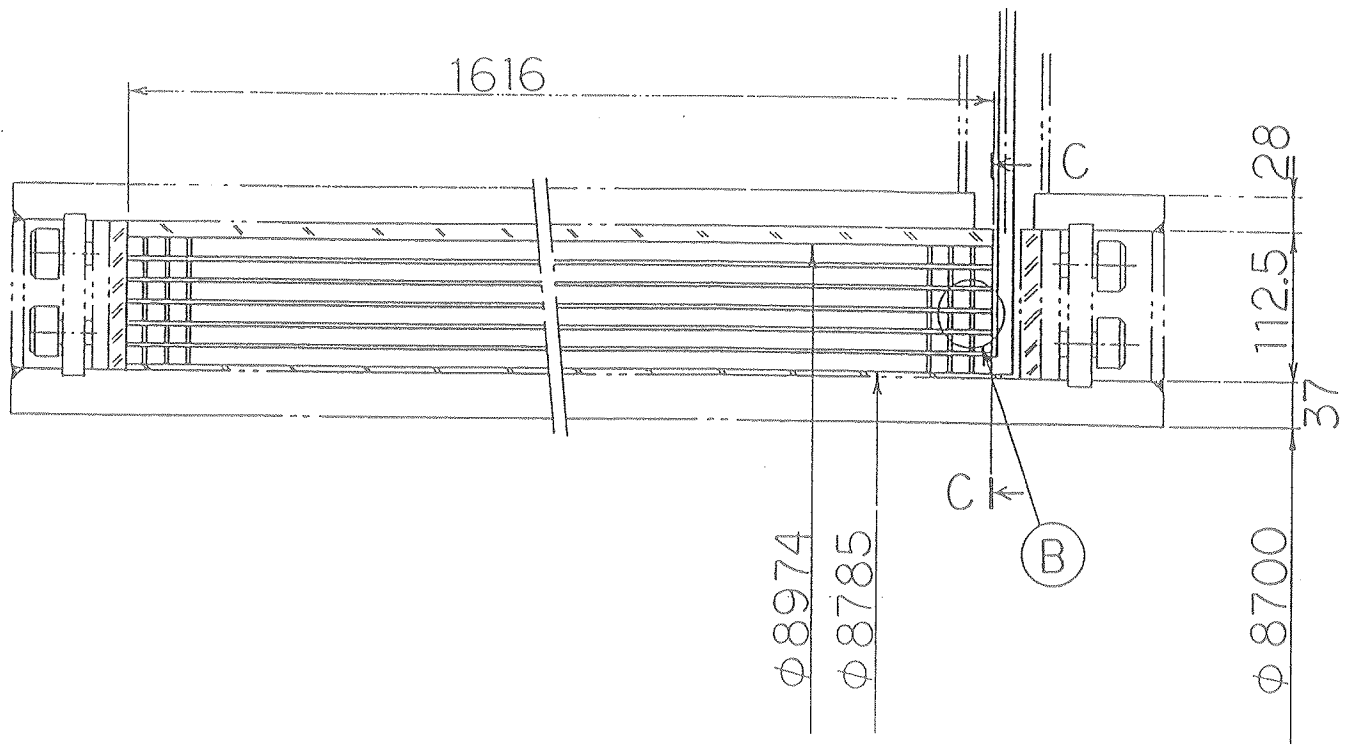


Figure 3-9.

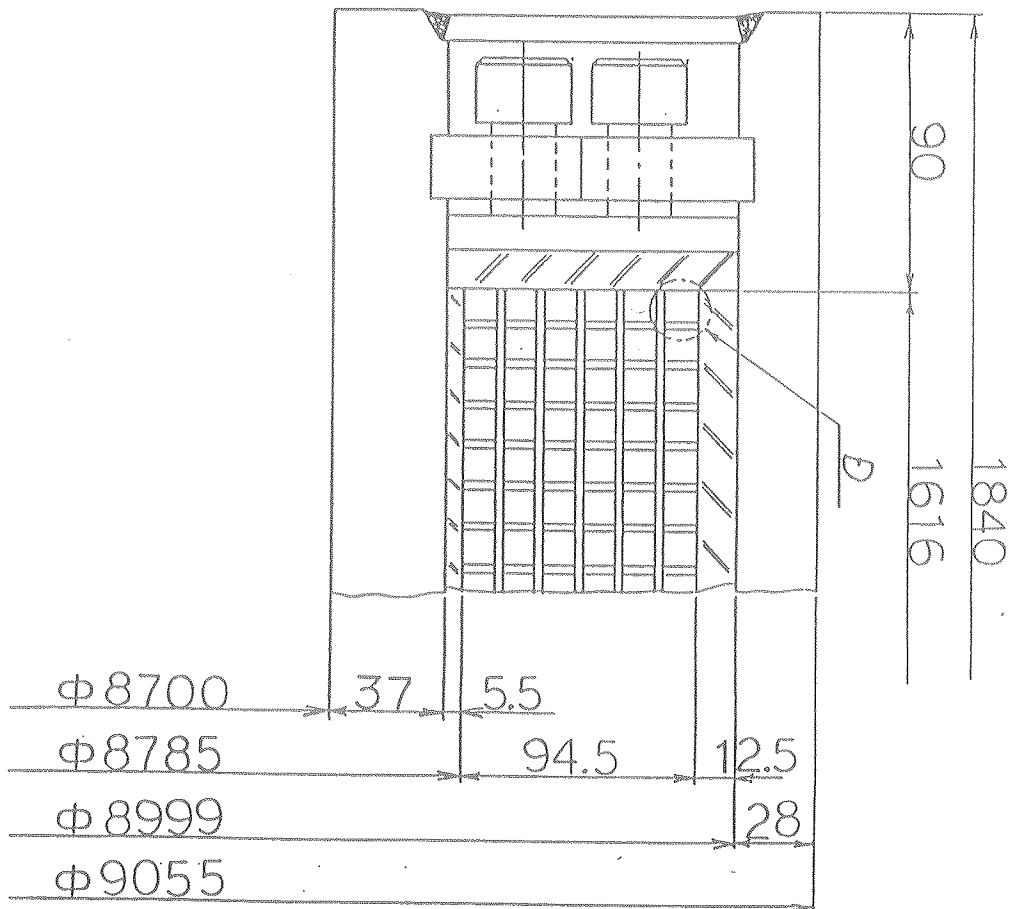
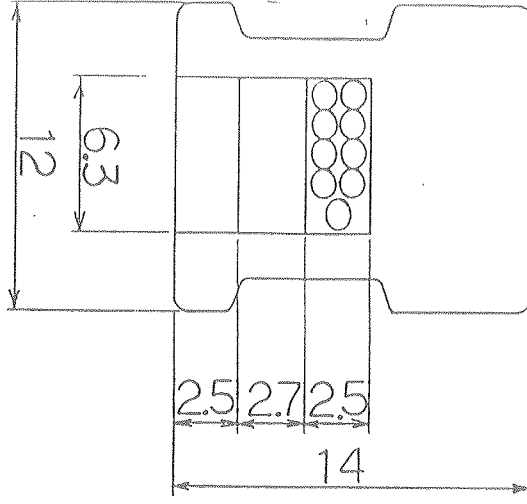


Figure 3-10.

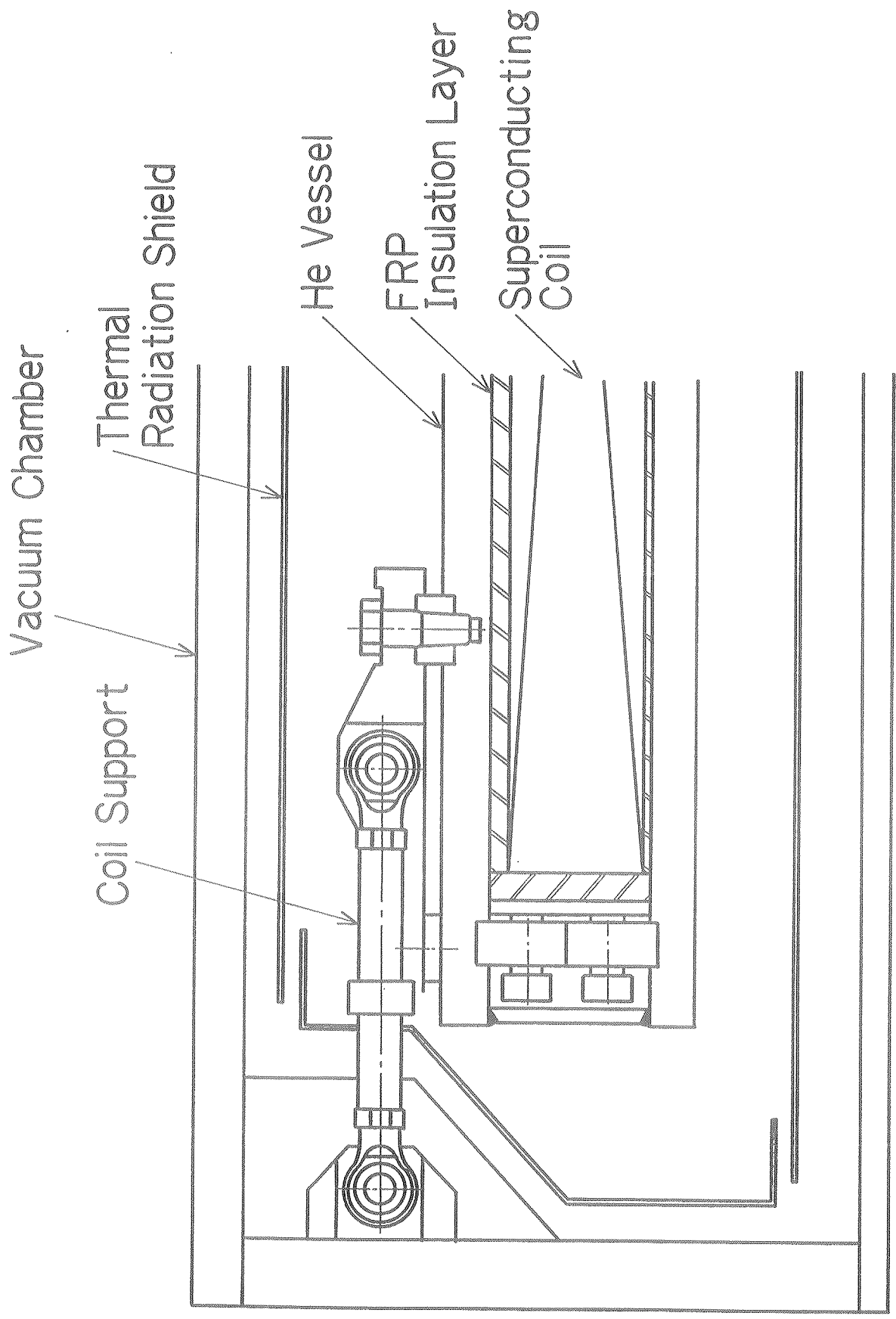


Figure 3-11.

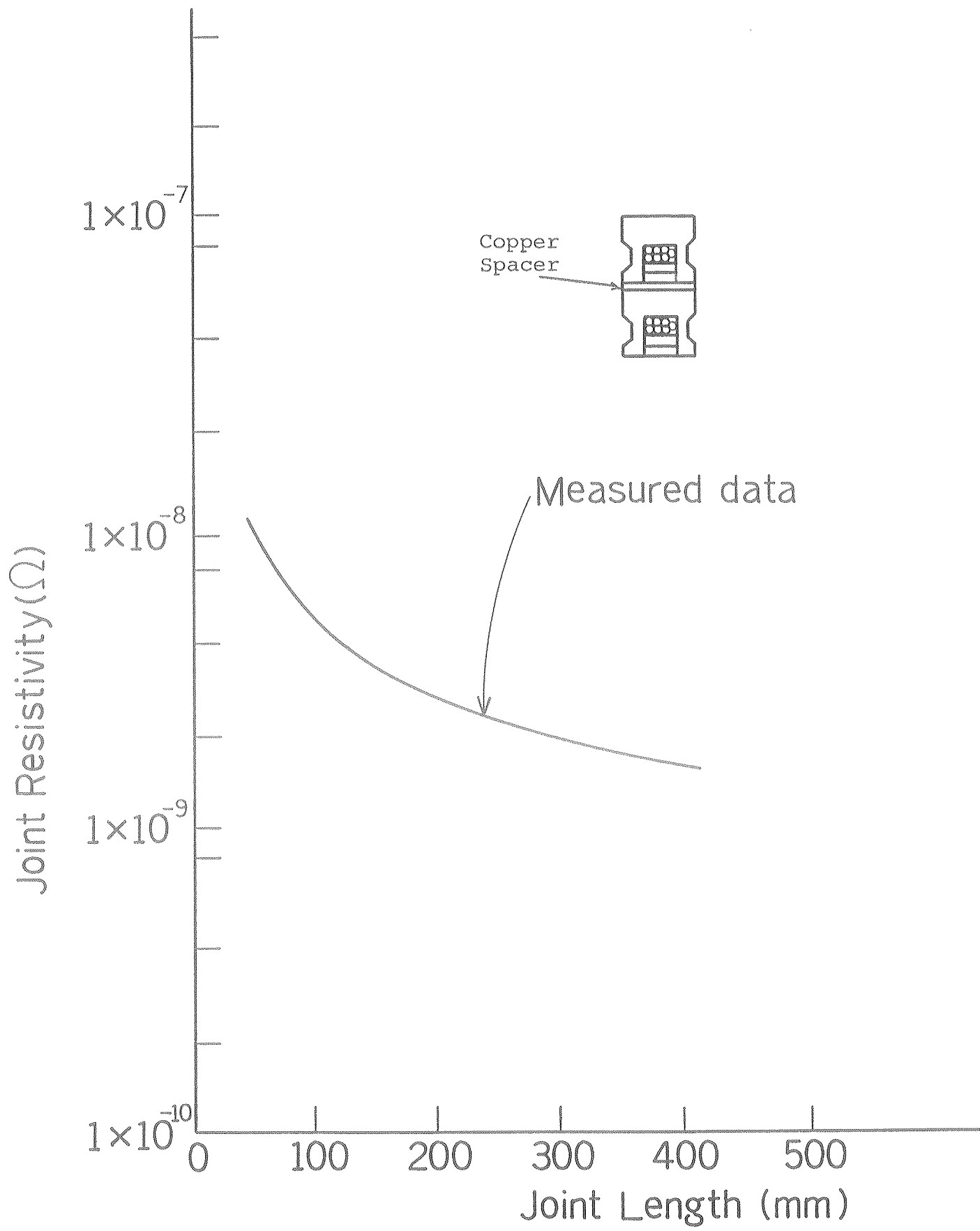


Figure 3-12.

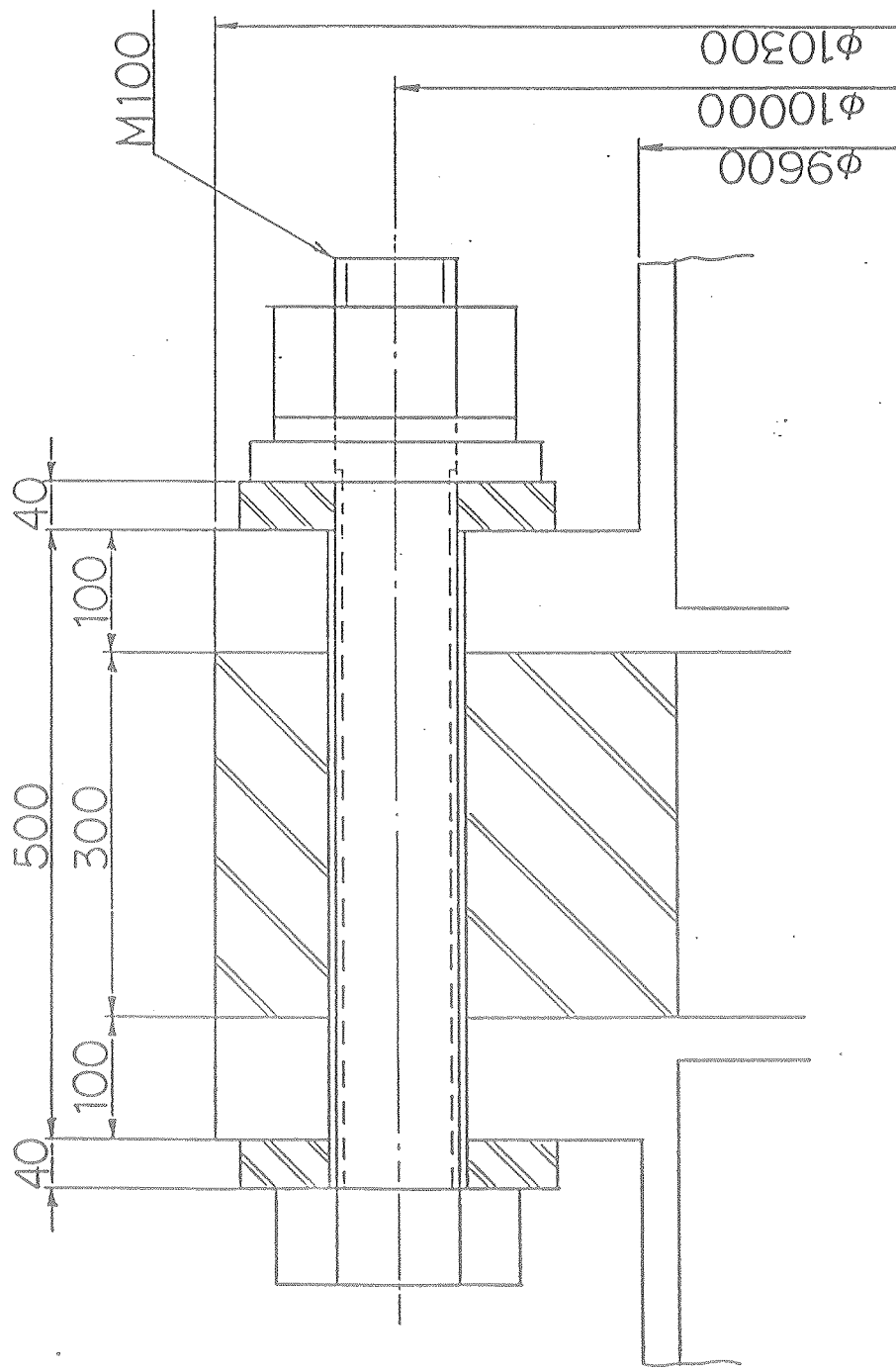
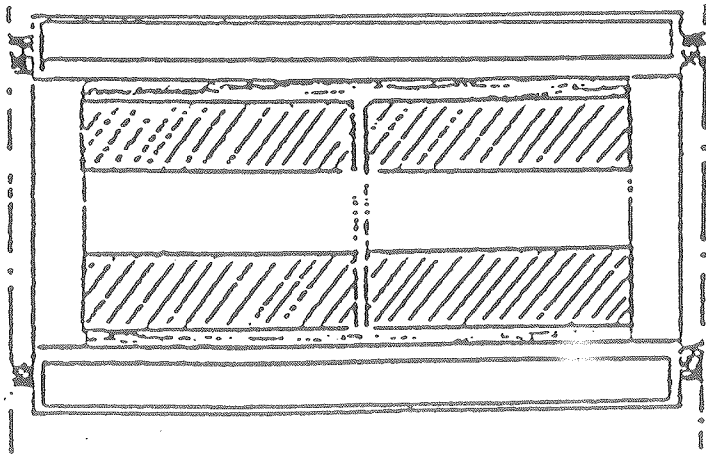
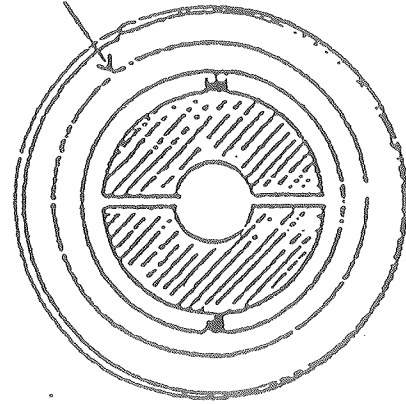


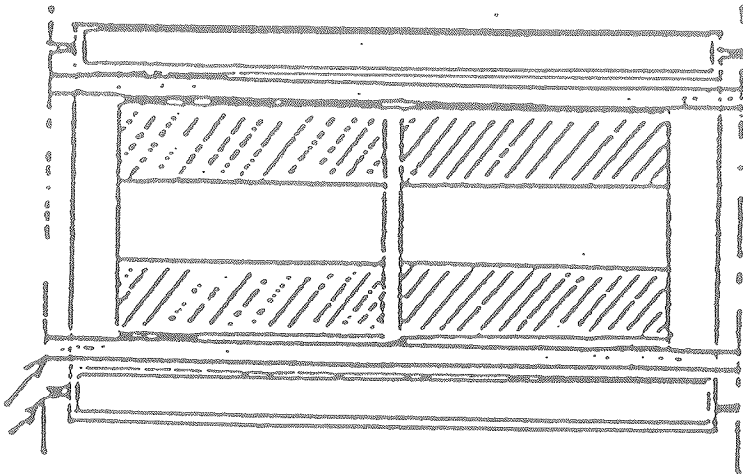
Figure 3-13.



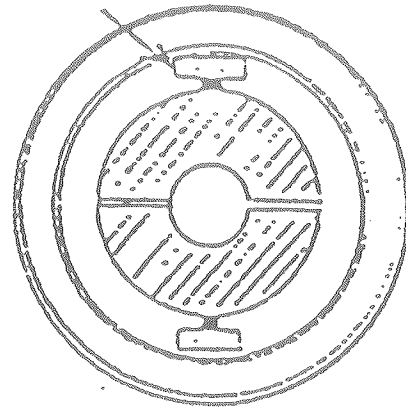
Cylinder support



(A) Cylinder Support



Pillar support



(B) Pillar Support

Figure 4-1.

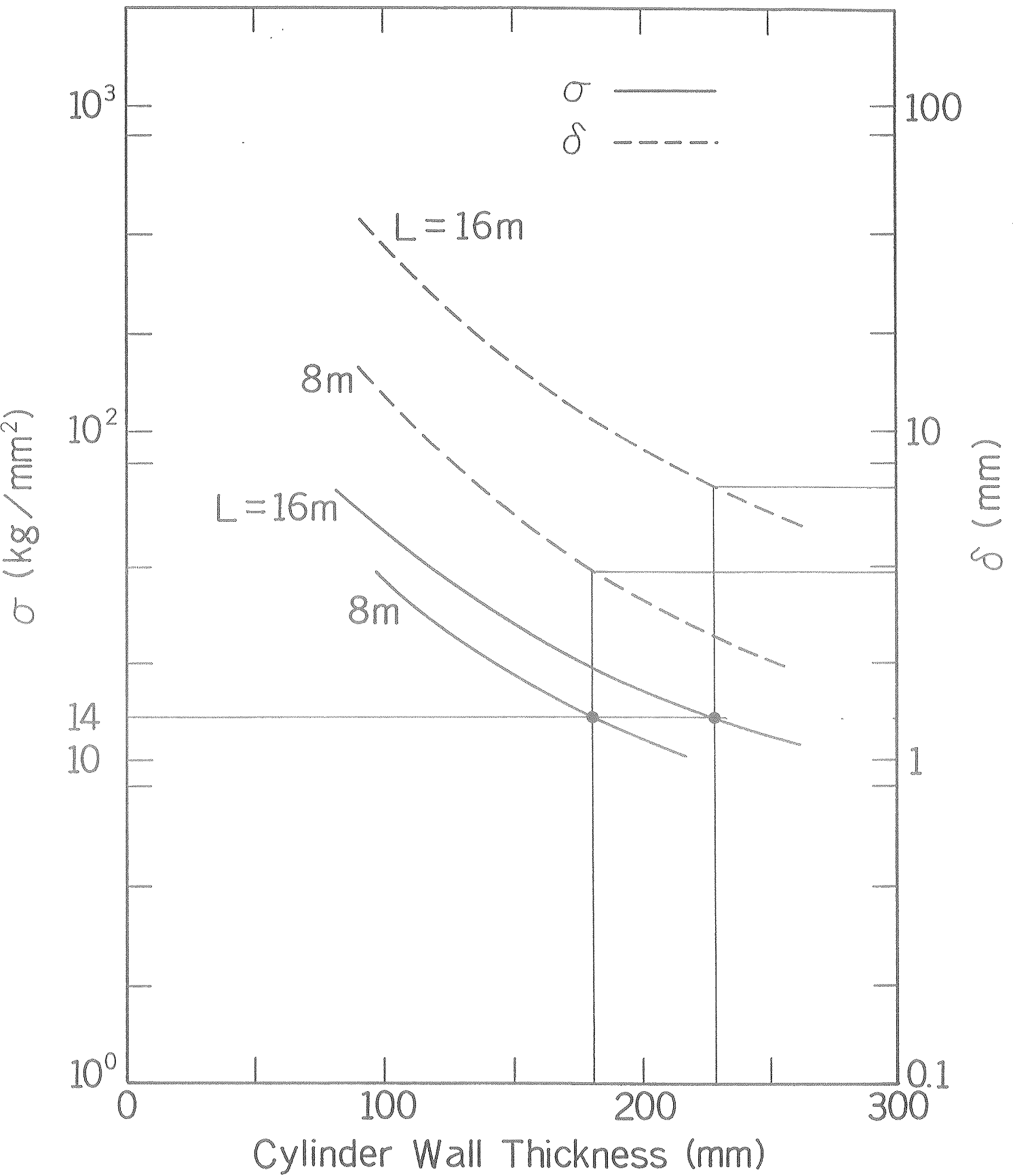


Figure 4-2.

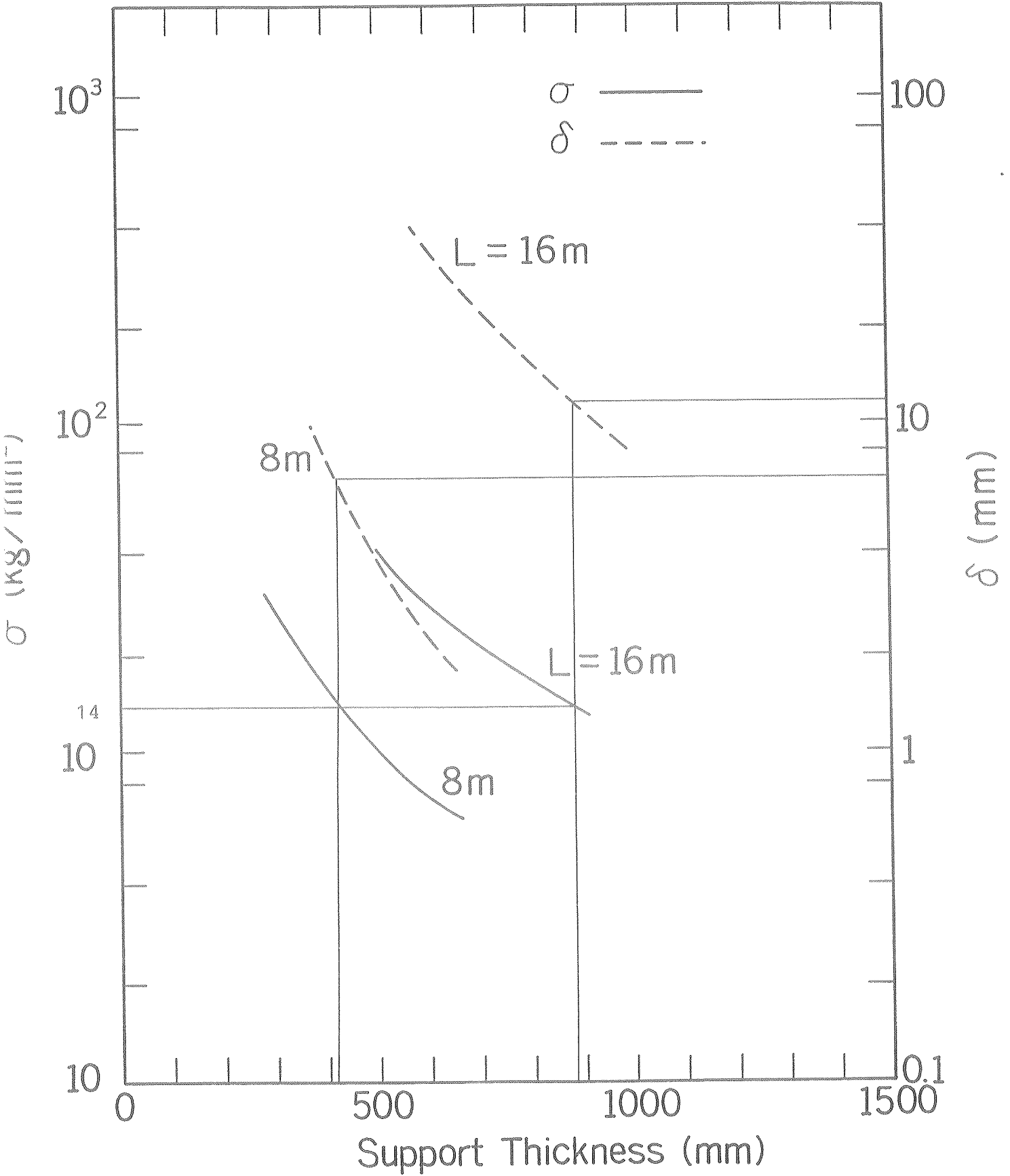


Figure 4-3.

Axial Support

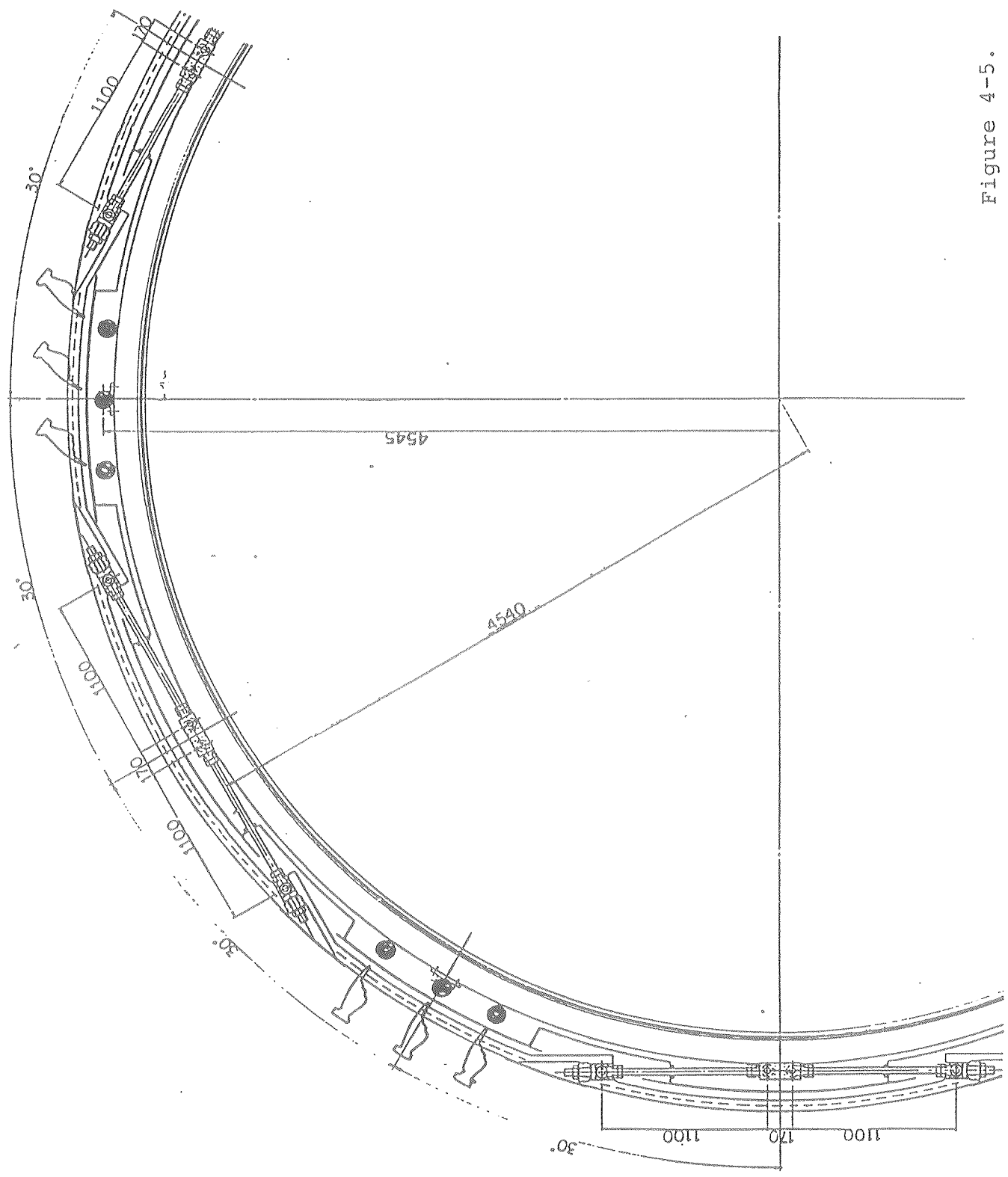


Figure 4-5.

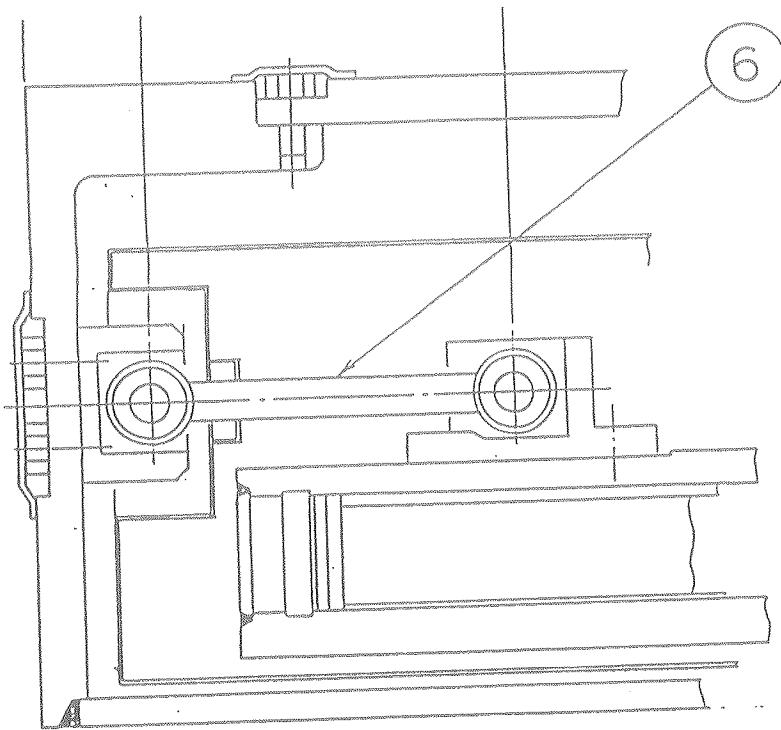
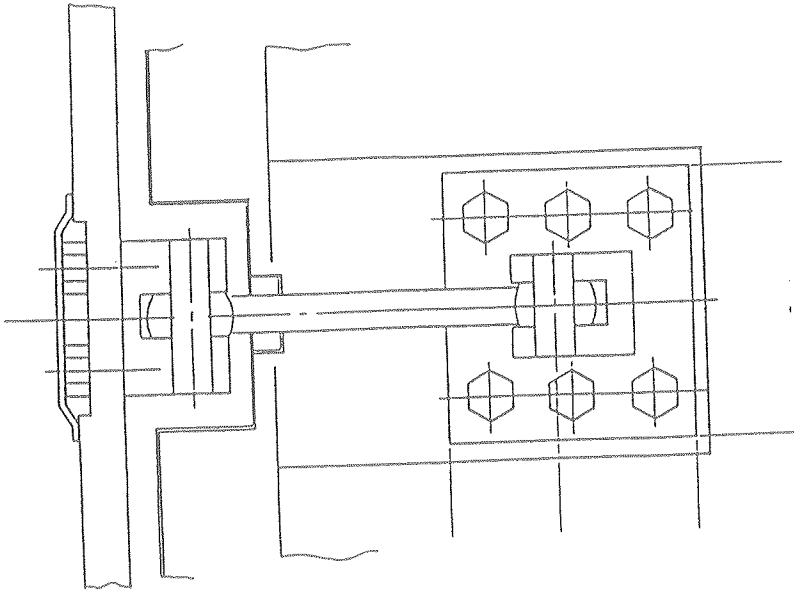


Figure 4-6.

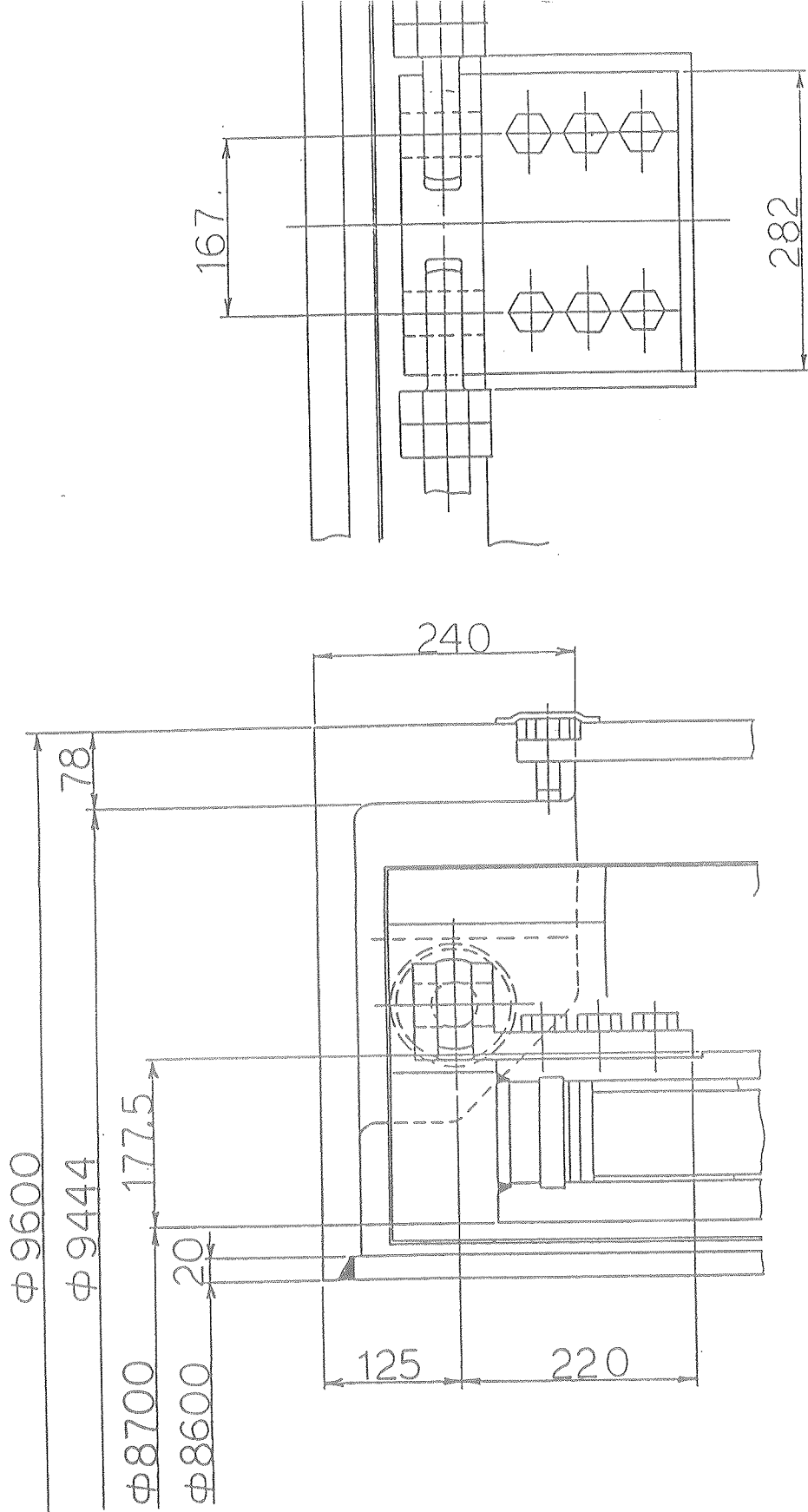


Figure 4-7.

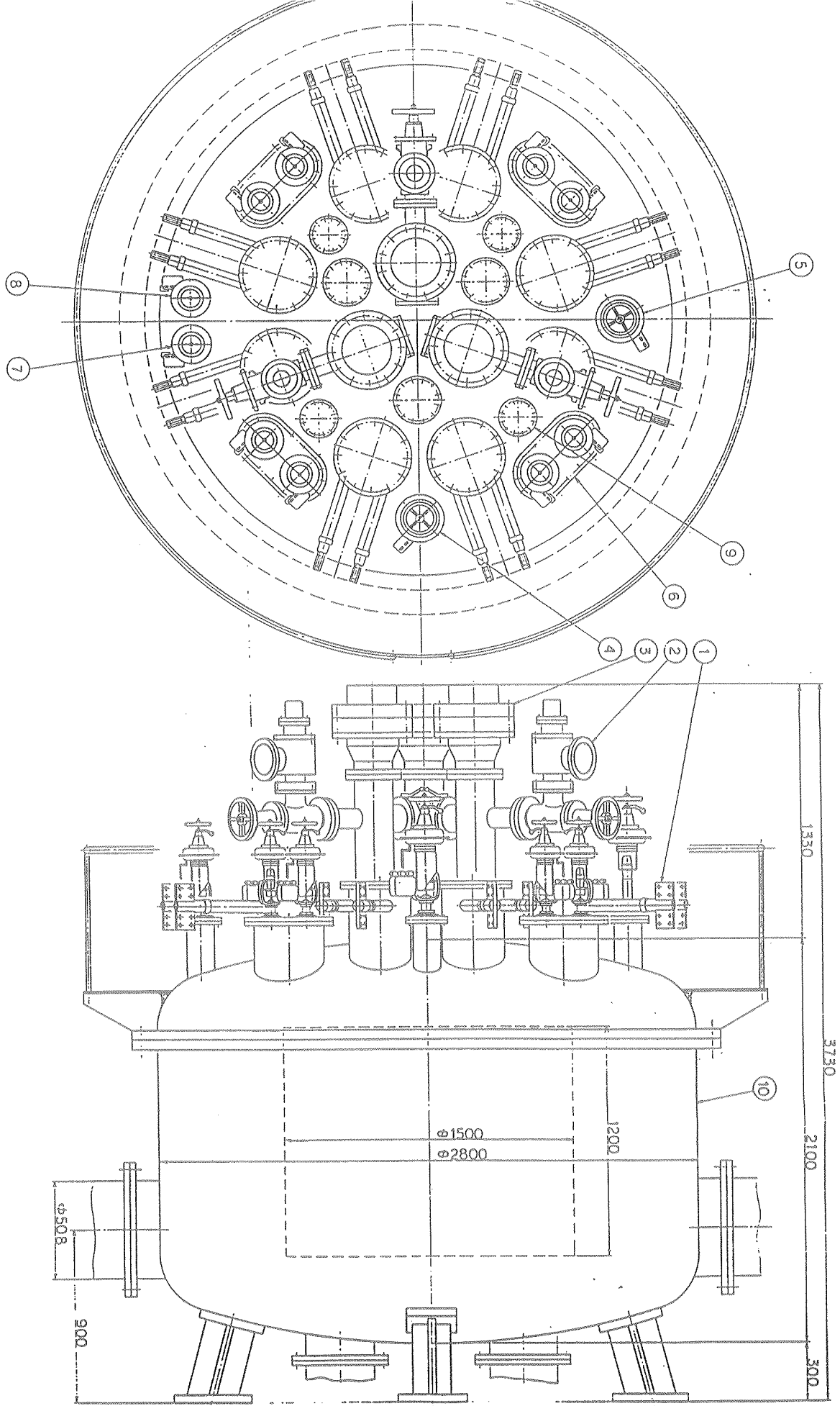
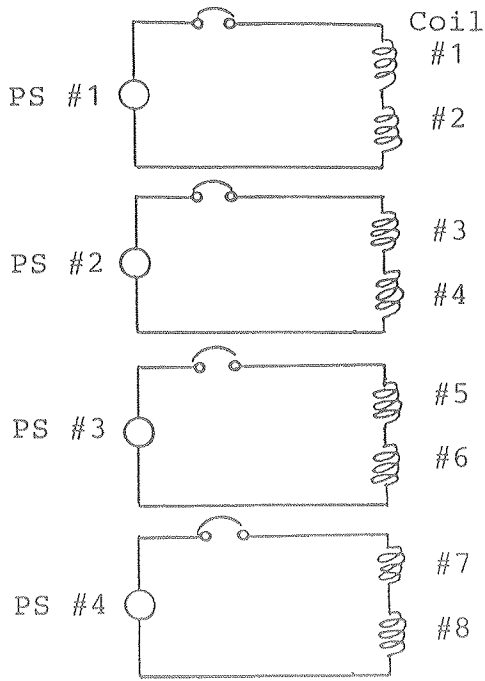
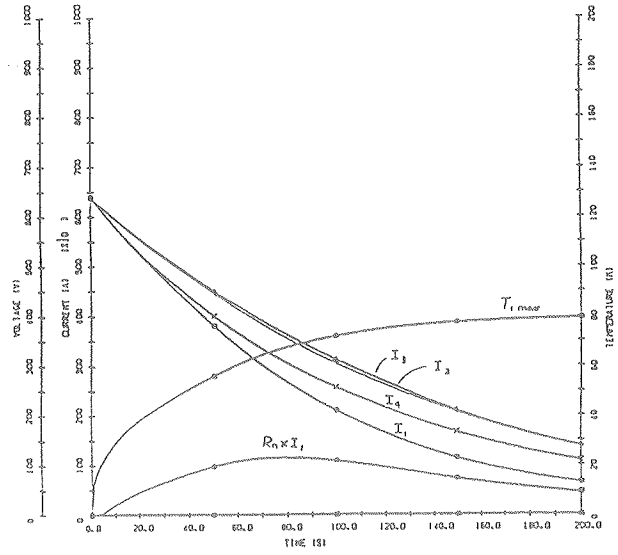


Figure 4-8.

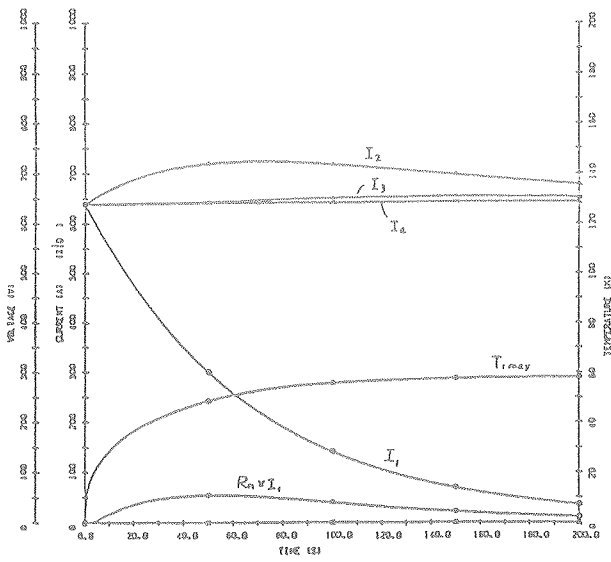
Dump Switch



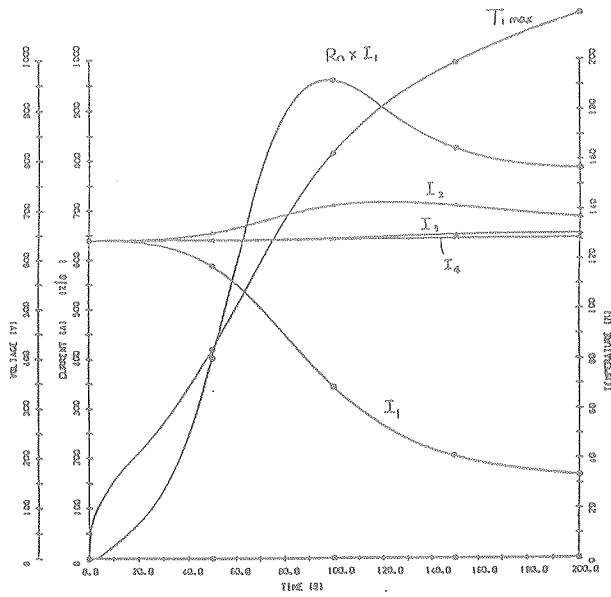
(a)



(b)



(c)



(d)

Figure 5-1.

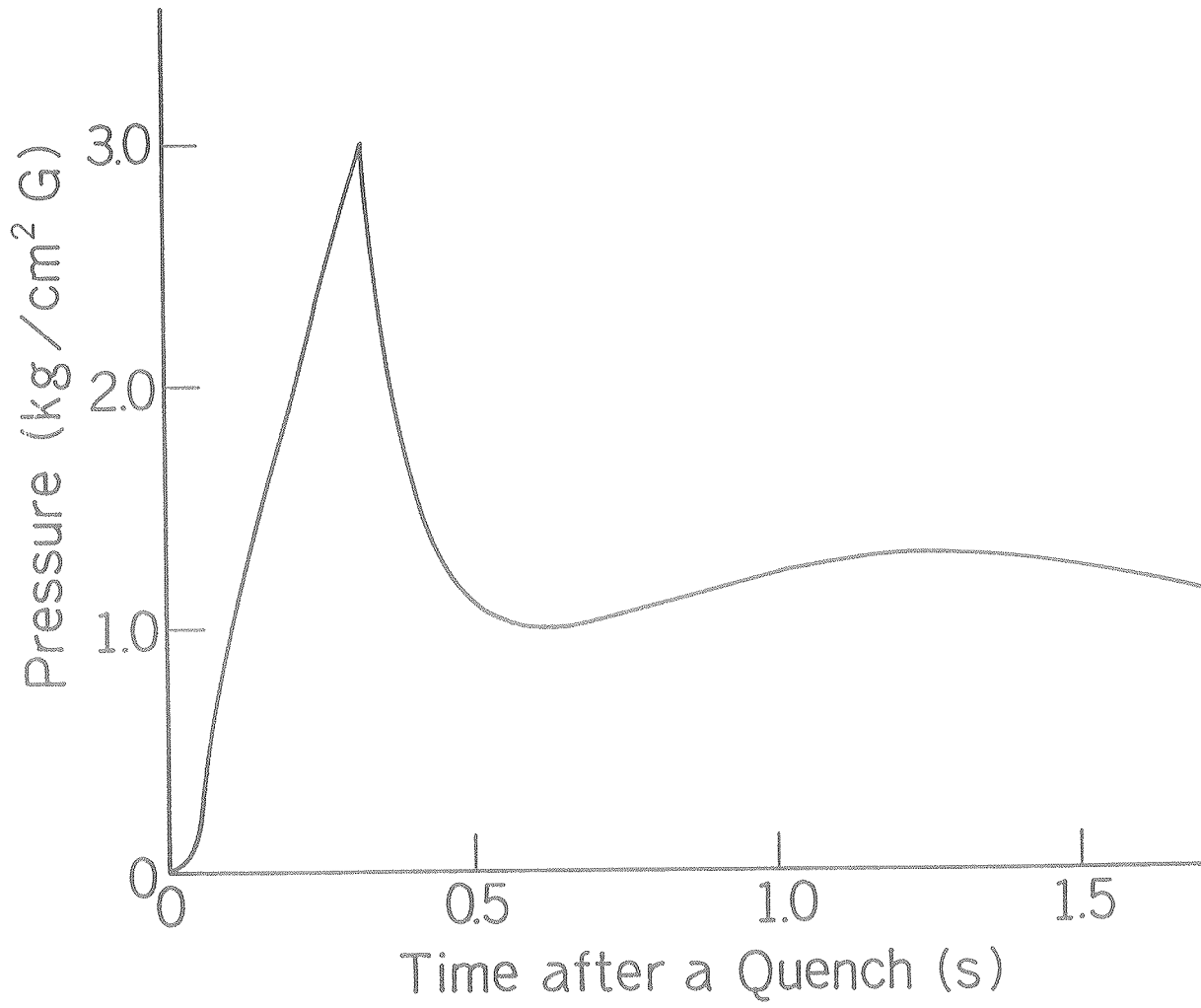


Figure 5-2.

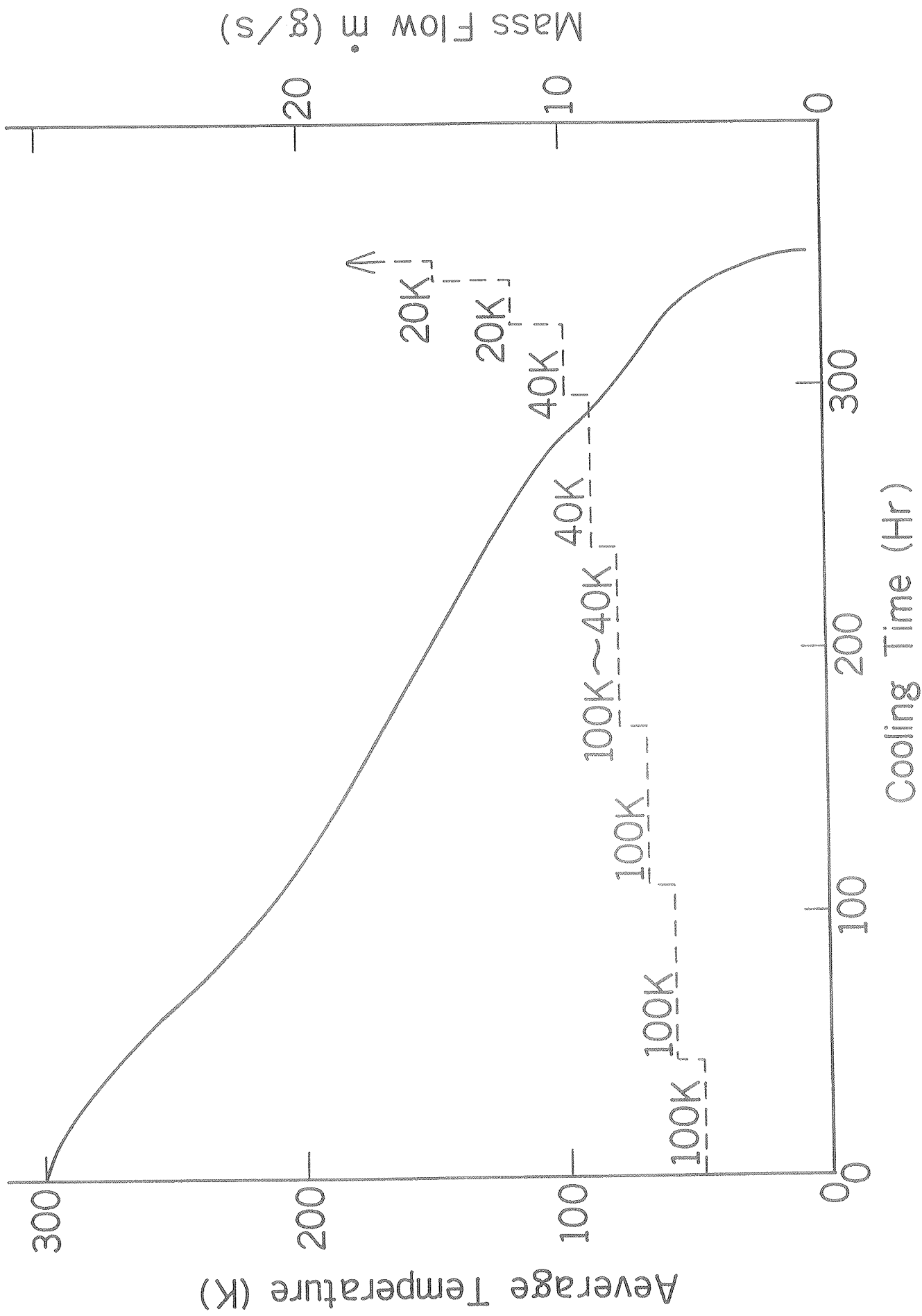


Figure 6-1.

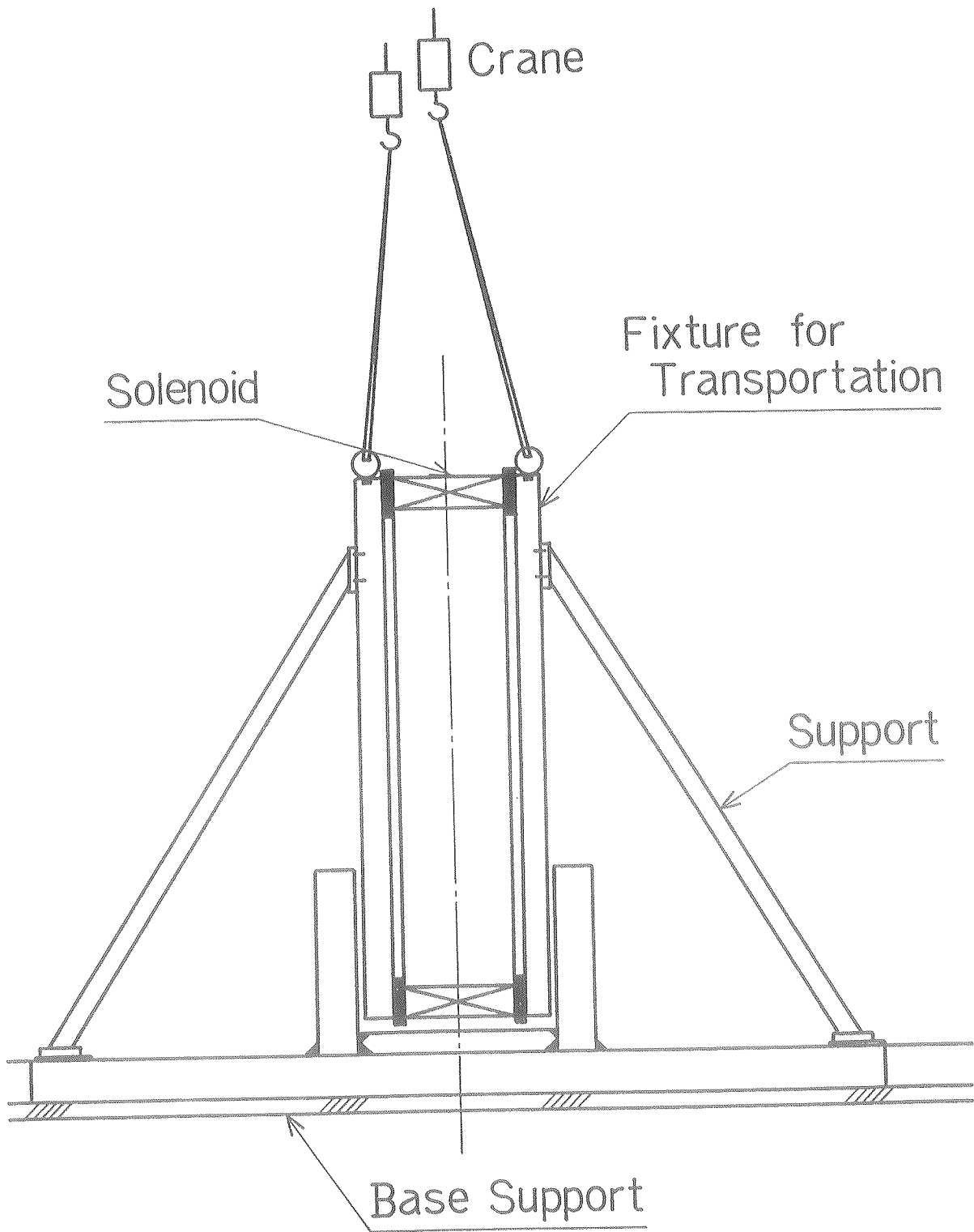


Figure 6-2.

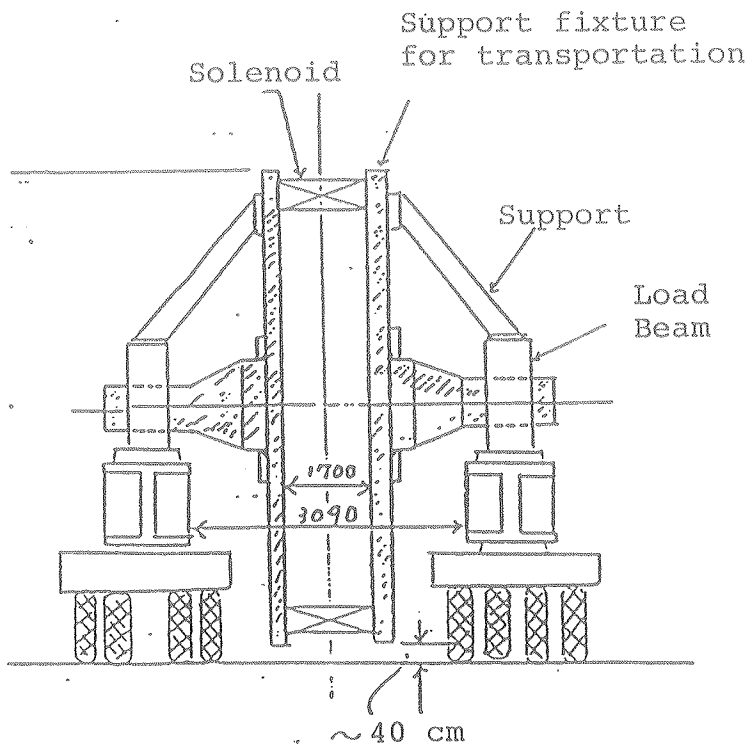
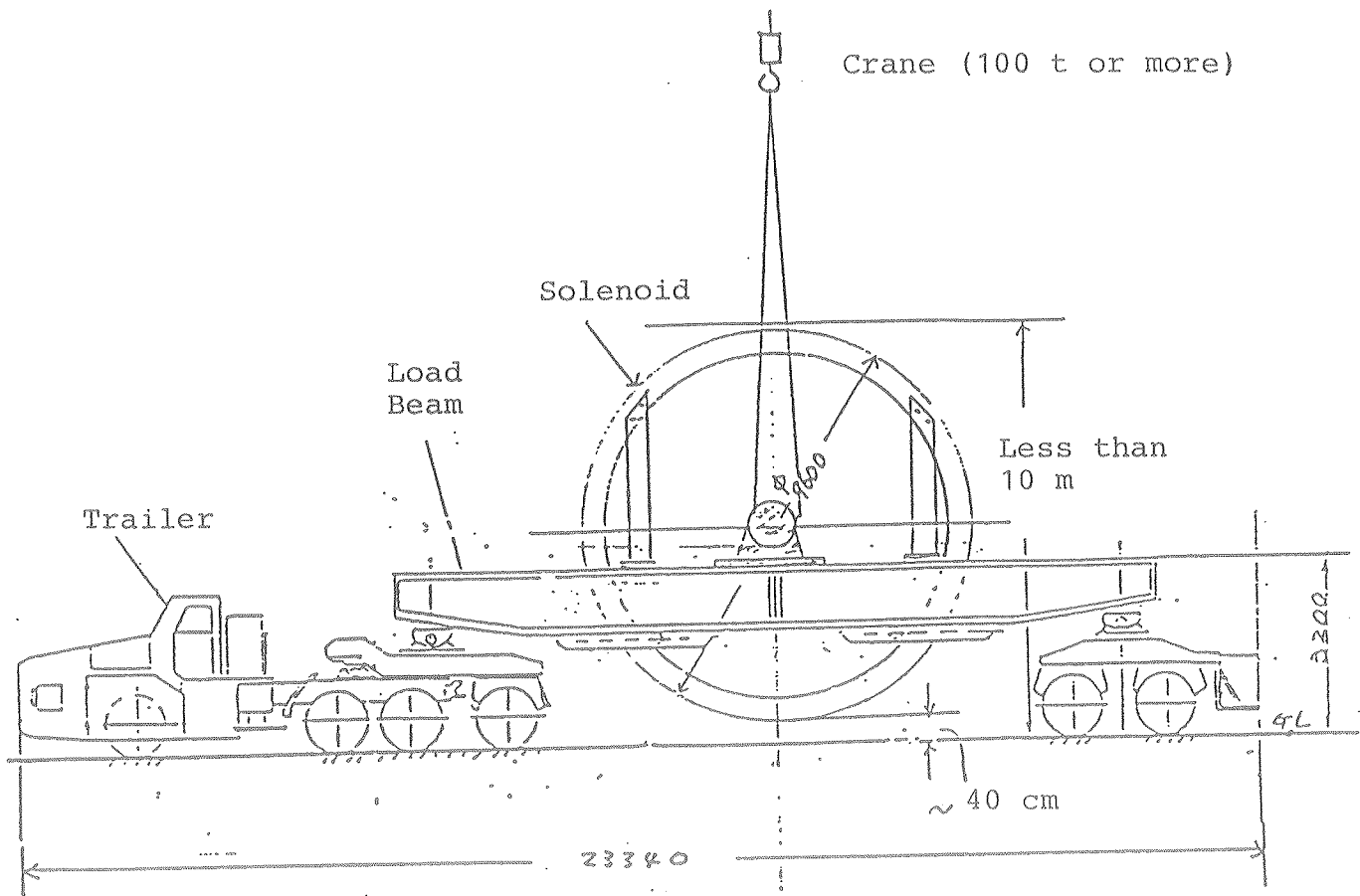


Figure 6-3.

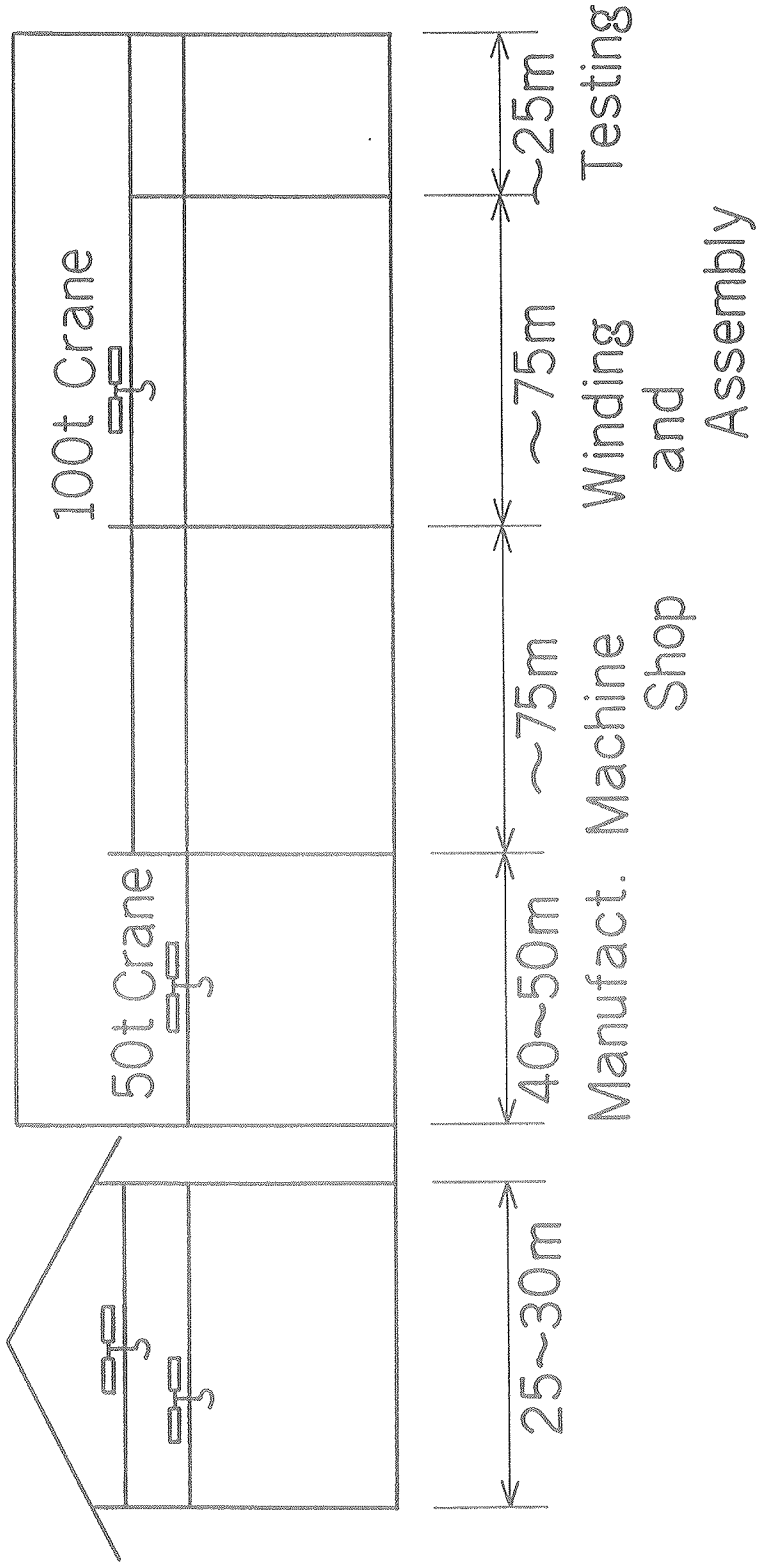


Figure 6-4.